(4)

Quarterly Letter Report

Growth, Characterization and Device Development in Monocrystalline Diamond Films

Supported by the Innovative Science and Technology Office
Strategic Defense Initiative Organization
Office of Naval Research
under Contract #N00014-90-J-1604
for the period July 1, 1992–September 30, 1992

R. F. Davis, J. T. Glass, R. J. Nemanich* and R. J. Trew**
L. Bergman*, B. R. Stoner, K. F. Turner* and S. Wolter
North Carolina State University
c/o Materials Science and Engineering Department
*Department of Physics
**Electrical and Computer Engineering
Raleigh, NC 27695

September 30, 1992

REPORT DOCUMENTATION PAGE

Form Approved
OMB No 0704 0188

1. AGENCY USE ONLY (Leave Blank)	2. REPORT DATE	3. REPORT TYPE AND DATES COVERED
	September 1992	Quarterly Letter 7/1/92—9/30/92

4. TITLE AND SUBTITLE

Growth, Characterization and Device Development in Monocrystalline Diamond Films

5. FUNDING NUMBERS

s400003srr08
1114SS
N00179
N66005
4B855

6. AUTHOR(S)

Robert F. Davis

7. PERFORMING ORGANIZATION NAME(S) AND ADDRESS(ES)

North Carolina State University
Hillsborough Street
Raleigh, NC 27695

8. PERFORMING ORGANIZATION REPORT NUMBER

N00014-90-J-1604

9. SPONSORING/MONITORING AGENCY NAME(S) AND ADDRESS(ES)

Department of the Navy
Office of the Chief of Naval Research
800 North Quincy Street, Code 1513:CMB
Arlington, VA 22217-5000

10. SPONSORING/MONITORING AGENCY REPORT NUMBER

11. SUPPLEMENTARY NOTES

12a. DISTRIBUTION/AVAILABILITY STATEMENT

Approved for Public Release—Distribution Unlimited

12b. DISTRIBUTION CODE

13. ABSTRACT (Maximum 200 words)

Ordered diamond films have been deposited on single crystal Si(100) substrates via in-situ carburization followed by bias-enhanced nucleation. Photoluminescence and Raman spectroscopy have been employed to determine the time evolution of defect formation in these CVD diamond films for stages of growth spanning nucleation to continuous film formation. Analysis of the 1332 cm^{-1} diamond feature showed two rates of diamond growth with a transition at the thickness where nearly complete coverage was obtained. Investigation of the various defects in the films led to the conclusions that Si atoms most likely caused the 1.68 eV optical centers at the initial stages of growth. Luminescence associated with sp^2 bonding defects appeared only after a continuous film was formed. The CVD growth of diamond films on Si (100) have also been studied using scanning tunneling spectroscopy. The surface of the diamond film possessed electronic structure similar to single crystal diamond. By contrast the initial growth surface showed evidence of β-SiC and graphite electronic structures. The microwave performance of p-type diamond MESFETs is also under investigation. The surface breakdown model has been further refined and an activation model has been included so that free charge density as a function of temperature could be determined. Research is also underway to simulate the performance of the Kobe p-channel MESFET. A pn junction gate model is also being formulated so that the operation of a diamond JFET can be investigated.

14. SUBJECT TERMS	15. NUMBER OF PAGES
diamond thin films, silicon carbide, heteroepitaxial nucleation, misfit dislocations, interfacial strain energy, plasma cleaning, negative electron affinity, atomic hydrogen, argon plasma, uv photoemission	69
	16. PRICE CODE

17. SECURITY CLASSIFICATION OF REPORT	18. SECURITY CLASSIFICATION OF THIS PAGE	19. SECURITY CLASSIFICATION OF ABSTRACT	20. LIMITATION OF ABSTRACT
UNCLAS	UNCLAS	UNCLAS	SAR

Table of Contents

I. Introduction

Diamond as a semiconductor in high-frequency, high-power transistors has unique advantages and disadvantages. Two advantages of diamond over other semiconductors used for high-frequency, high-power devices are its high thermal conductivity and high electric-field breakdown. The high thermal conductivity allows for higher power dissipation over similar devices made in Si or GaAs, and the higher electric field breakdown makes possible the production of substantially higher power, higher frequency devices than can be made with other commonly used semi-conductors.

In general, the use of bulk crystals severely limits the potential semiconductor applications of diamond. Among several problems typical for this approach are the difficulty of doping the bulk crystals, device integration problems, high cost and low area of such substrates. In principal, these problems can be alleviated via the availability of chemically vapor deposited (CVD) diamond films. Recent studies have shown that CVD diamond films have thermally activated conductivity with activation energies similar to crystalline diamonds with comparable doping levels. Acceptor doping via the gas phase is also possible during activated CVD growth by the addition of diborane to the primary gas stream.

The recently developed activated CVD methods have made feasible the growth of polycrystalline diamond thin films on many non-diamond substrates and the growth of single crystal thin films on diamond substrates. More specifically, single crystal epitaxial films have been grown on the {100} faces of natural and high pressure/high temperature synthetic crystals. Crystallographic perfection of these homoepitaxial films is comparable to that of natural diamond crystals. However, routes to the achievement of rapid nucleation on foreign substrates and heteroepitaxy on one or more of these substrates has proven more difficult to achieve. This area of study has been a principal focus of the research of this contract.

At present, the feasibility of diamond electronics has been demonstrated with several simple experimental devices, while the development of a true diamond-based semiconductor materials technology has several barriers which a host of investigators are struggling to surmount. It is in this latter regime of investigation that the research described in this report has and continues to address.

The principal vectors of the research in this reporting period have been (1) the deposition of diamond films on single crystal Si(100) substrates via *in-situ* carbonization followed by bias-enhanced nucleation, (2) the photoluminescence and Raman spectroscopy of the defects of CVD diamond on Si(100), (3) the scanning tunneling spectroscopy of the initial and final growth surfaces and (4) modeling of simulated diamond MESFET structures.

The following subsections detail the experimental procedures for each of the aforementioned studies, discuss the results and provide conclusions and references for these studies. Note that each major section is self-contained with its own figures, tables and references.

II. Textured Growth of Diamond on Silicon via In-situ Carburization and Bias-enhanced Nucleation

S.D. Wolter, B.R. Stoner, and J.T. Glass
Department of Materials Science and Engineering
North Carolina State University
Raleigh, NC 27695-7919 USA

P.J. Ellis, D.S. Buhaenko, C.E. Jenkins and P. Southworth
Kobe Steel Europe Laboratory
Surrey Research Park
Guildford, England UK

Abstract

Ordered diamond films have been deposited on single crystal silicon substrates via an in-situ carburization followed by bias-enhanced nucleation. Textured diamond films with greater than 30% of the grains oriented D(100)//Si(100) and D<110>//Si<110> were grown in both a horizontal and vertical microwave plasma chemical vapor deposition reactor. Separate diamond films from each of the two reactors were analyzed both by scanning electron microscopy and Raman spectroscopy. The in-situ carburization is speculated to form an epitaxial SiC conversion layer, thus providing an economical alternative to obtaining epitaxial diamond films on single crystal SiC.

The nucleation and growth of heteroepitaxial diamond films is of prime interest if the scientific community is to take full advantage of this material's extreme and unique properties[1]. It is therefore important to develop a technique to accommodate this objective as well as make it economically viable. Diamond films have been epitaxially deposited on both diamond [2] and c-BN [3-5] single crystal substrates providing evidence that at typical low-pressure processing conditions single crystal diamond deposition is possible. It is understandable that depositing monocrystalline diamond films on substrates other than diamond or cBN would be more advantageous due to the extreme difficulty in obtaining large single crystals of either of these materials.

Recent success in obtaining textured diamond growth on β-SiC[6] has presented a novel approach to heteroepitaxy. This approach termed bias-enhanced diamond nucleation was originally found to enhance the number of stable diamond nuclei on Si(100) substrates[7, 8]. The conventional diamond-scratching procedure used to promote nucleation was thus eliminated making it possible to nucleate diamond on pristine substrates. Texturing was not observed in the original bias-enhanced nucleation studies on Si(100) substrates [9], due in part to the formation of an amorphous SiC interfacial layer thus leading to randomly oriented diamond particles. In the present study, however, the bias-pretreatment is preceded by a carburization step that is speculated to form an epitaxial conversion layer of β-SiC on Si.

Evidence has been provided through past work that under appropriate processing conditions the formation of an epitaxial conversion layer of β-SiC on Si is possible. Williams et al.[10] reported transmission electron microscopy (TEM) results of an epitaxial β-SiC buffer layer and local twinned epitaxy of diamond that was formed during diamond growth on Si. In another study, localized epitaxy of diamond on Si was reported by Jeng et al.[11] and may have also

resulted from the formation of an epitaxial β-SiC buffer layer. In the latter study textured particles were reportedly observed via scanning electron microscopy, however, an in depth analysis was not performed and complete films were not obtained. It is the purpose of this letter to report the nucleation and subsequent growth of oriented diamond films on Si(100) substrates that were first pretreated by an in-situ carburization step followed immediately by bias-enhanced nucleation. Until high quality single crystal SiC substrates become economically available, this two-step pretreatment process may provide a reasonable alternative for obtaining highly textured diamond films on non-diamond substrates.

The low-pressure diamond growth was performed on Si(100) substrates via microwave plasma chemical vapor deposition (MPCVD) involving the following three-step process; (i) carburization, (ii) biasing, and (iii) deposition. The carburization and biasing steps may be viewed as in-situ pretreatment routines; the carburization step used to grow an epitaxial SiC conversion layer followed by the biasing step used to promote the formation of stable diamond nuclei. No scratching or conventional form of nucleation enhancement was utilized. The deposition step involved the optimum conditions for growth on the pre-existing diamond nuclei.

The three-step growth process was performed using two separate MPCVD reactors, purchased in part from Applied Science Technology, Inc. (ASTeX). The chambers were six inch inner diameter stainless steel resonant cavities; one in a vertical and the other in a horizontal configuration. The vertical reactor was used at Kobe Steel European Laboratory (KSEL) in the UK and the horizontal configuration was used at North Carolina State University (NCSU). The vertical reactor utilized ASTeX's standard 4-inch diameter induction heated substrate holder and was modified with a high voltage, medium current electrical

feedthrough to allow for independent substrate biasing. A complete description of the horizontal growth chamber as well as the biasing set-up used during the bias-enhanced nucleation step have been previously published[9]. Briefly, the substrate rests in a two-inch diameter slotted molybdenum substrate holder that fits onto an electrically isolated, resistively heated tantalum can. An electrical lead connected to the tantalum can allows for independent substrate biasing.

The three processing steps mentioned above were slightly different for the two separate reactors and are listed in Table 1. Described in detail below are the processing procedures for the vertical reactor. The Si(100) substrates were etched in dilute HF acid and thoroughly rinsed in de-ionized water prior to insertion into the growth chamber. The carburization step was undertaken for 1 hour at 2% CH4/H2 with a chamber pressure of 25 torr. The microwave power was 1200 Watts and the substrate was immersed roughly 0.5 cm into the plasma. The temperature during this step was maintained between 900-930°C as measured by a single color optical pyrometer. The bias step was performed immediately following the carburization, where the ambient pressure was reduced to 15 torr and the CH4/H2 ratio was increased to 5%. In addition, the substrate was moved to the edge of the plasma (i.e. 0 cm downstream). A bias-potential of -250 VDC was then applied to the substrate, inducing a current of approximately 100-140mA. The total length of biasing was approximately 3 minutes. Following the biasing step, the substrate voltage was terminated and the substrate was moved 0.4 cm downstream from the plasma. The pressure was raised to 25 torr with a CH_4/H_2 ratio of 0.5%. The substrate temperature for both the biasing and growth step was between 700-750°C.

Several analytical techniques were used to characterize the diamond that was deposited via this three step process. Scanning electron microscopy (SEM) and Raman spectroscopy were used to investigate the morphology and quality of

the diamond, respectively. Auger electron spectroscopy (AES) was also performed, in-vacuo, to analyze the substrate surface following the carburization step in the horizontal reactor.

It has been observed that by reducing the total length of biasing time a sufficiently high number of nuclei will be formed without damaging the existing diamond nuclei by prolonged exposure to the biasing[7, 8]. In the absence of the carburization step a biasing time of roughly 30 minutes was necessary to obtain a nucleation density sufficient to form a complete diamond film. The carburization step effectively reduced this biasing time to 15 minutes and eventually 3 minutes was found to be adequate for obtaining a relatively high number of diamond nuclei. AES was used to analyze the surface of the Si substrate following the carburization step and confirmed the presence of a silicon-carbide phase. The carburization step, therefore, serves two purposes; (i) to form an in-situ epitaxial carbide conversion layer as well as (ii) to reduce the nucleation incubation period and thus diminish the eroding effects of the biasing process.

Figures 1-a and -b show SEMs of diamond grown in the vertical reactor under the conditions listed in Table 1. In both micrographs there appear to be evidence of a preferred orientation. Figure 2 shows the center region of the film grown in the horizontal reactor and the arrow which points in the Si<110> direction indicates that a large percentage of the grains may be locally epitaxial with the Diamond(100)//Si(100) and the Diamond<110>//Si<110>. The SEMs indicate a higher percentage of azimuthal misorientation than was observed with the epitaxial nucleation of diamond on b-SiC[6]. A misorientation about the substrate normal, (001), and a tilt about the a <110> direction are evident here and were shown in a previous work to be a result of the high density of misfit dislocations at the interface, resulting from poor lattice matching[12]. Figure 3 shows the Raman spectra from the diamond film grown in the horizontal reactor.

The sharp peak at 1332 cm^{-1} indicates that the film is high quality diamond with a negligible graphitic component.

Bias-enhanced diamond nucleation has been shown to be an effective tool for the heteroepitaxial nucleation of diamond on β-SiC[6]. Biasing directly on silicon in the absence of a controlled carburization step, however, was observed previously to lead to the formation of randomly oriented particles.[9]. The approach taken in this study was to first deposit an epitaxial SiC layer followed by bias-enhanced diamond nucleation and then growth on the existing nuclei. The diamond particles nucleated in this study appear quite similar to the textured particles observed by Stoner et al. on the β-SiC substrates[6]. This suggests that an epitaxial SiC film of adequate quality is being deposited on which diamond may then epitaxially nucleate. The observations made in this study indicate that the quality and crystallinity of the carbide are critical in obtaining oriented diamond nuclei on Si substrates.

In conclusion, this letter has shown that oriented diamond grains may be nucleated on Si(100) substrates following an in-situ carburization and bias-enhancement. Textured films were deposited using this process in two different microwave plasma CVD reactors, in separate laboratories. Both processes resulted in a large percentage of the diamond grains having a preferred orientation relative to that of the silicon substrate. It was speculated that an epitaxial SiC conversion layer was grown during the carburization step and that subsequent diamond nucleation was epitaxial to the SiC. AES confirmed that SiC was formed on Si during the carburization step, however, future experiments involving transmission electron microscopy will be needed to confirm the crystallographic relationship between the diamond, SiC and Si.

Table 1: The three processing steps along with the conditions for each used by in two different reactor geometries

Parameters	Carburization		Bias		Growth
	Horizontal reactor	Vertical reactor	Horizontal reactor	Vertical reactor	Both reactors
Bias Voltage	0	0	-250VDC	-170VDC	0
Current	0	0	~100mA	~200mA	0
Time	1 hr.	1 hr.	3 min.	9 min.	>5 hrs.
CH4/H2	2%	2%	5%	2 %	0.5%
Pressure	25 torr	15 torr	15 torr	15 torr	25 torr
Microwave Power	1200 W	800 W	900 W	800 W	900 W
Substrate Temperature	~900°C	~800°C	~750°C	~700°C	600-700°C
Substrate Position	Immersed	Immersed	Immersed	Immersed	Remote

List of Figures

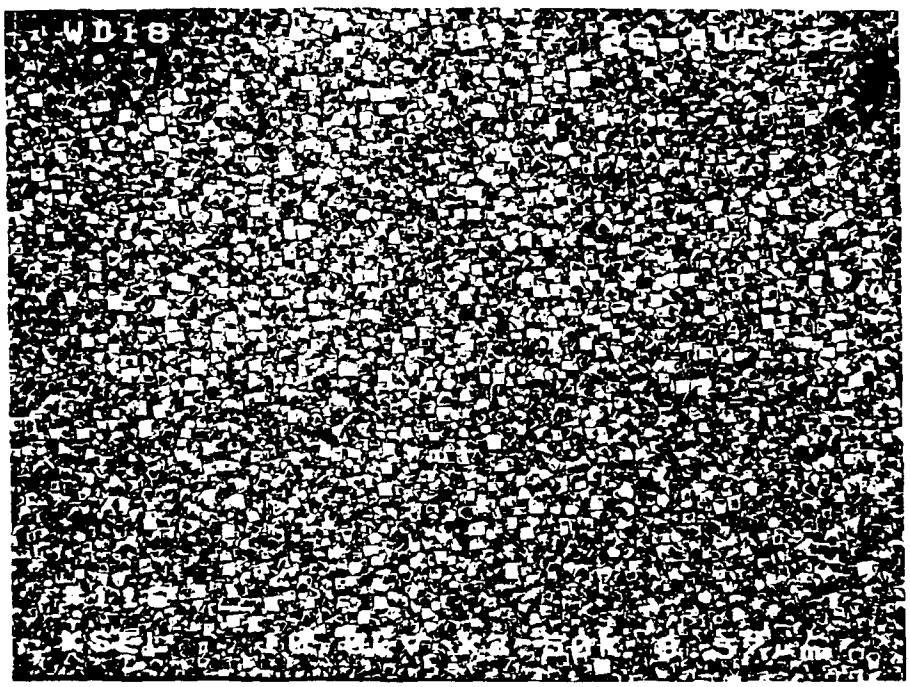

Figure 1a.

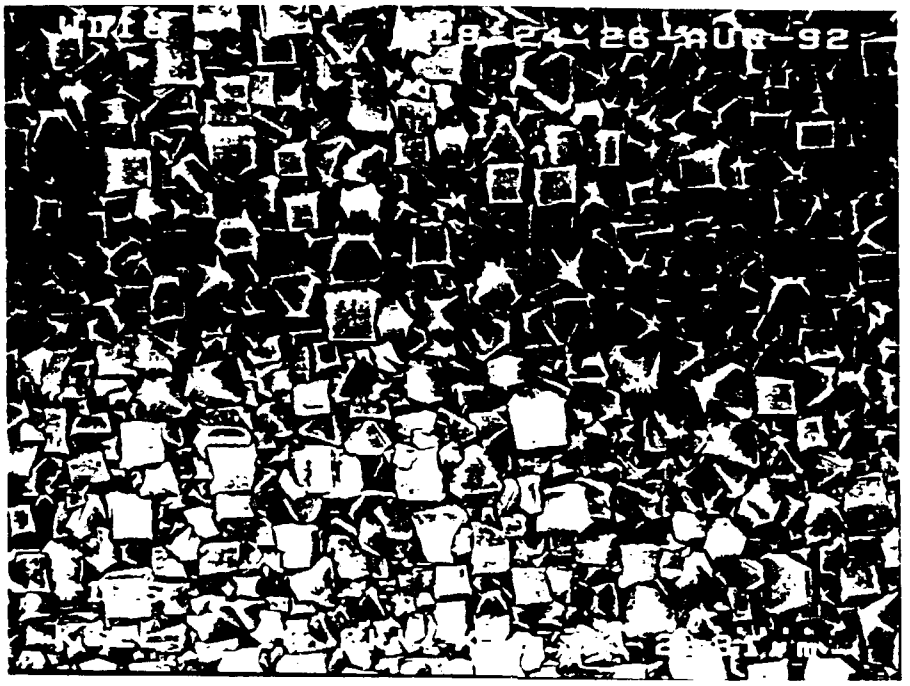

Figure 1b.

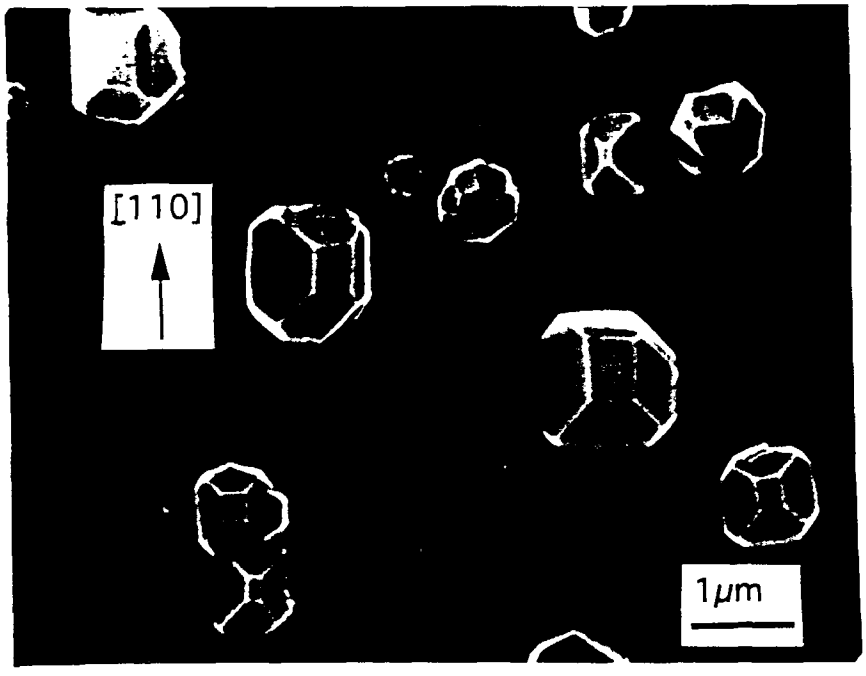

Figure 2.

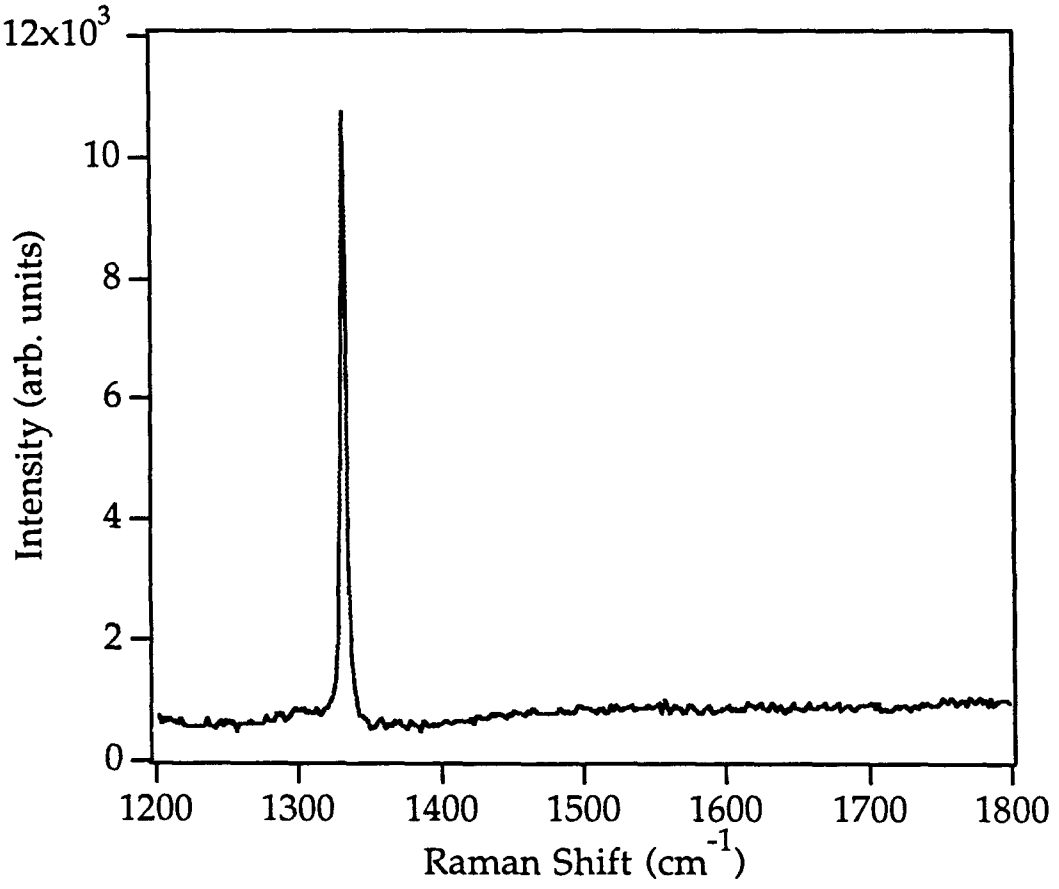
12x10^3
10
8
6
4
2
0
Intensity (arb. units)
1200
1300
1400
1500
1600
1700
1800
Raman Shift (cm^-1)

Figure 3.

References

1. W. A. Yarbrough, J. Vac. Sci. Technol. A, 9(3), 1145 (1991).

2. B. V. Spitsyn, L. L. Bouilov and B. V. Derjaguin, J. Cryst. Growth, 52(219 (1981).

3. S. Koizumi, T. Murakami, T. Inuzuka and K. Suzuki, Appl. Phys. Lett., 57(6), 563 (1990).

4. M. Yoshikawa, H. Ishida, A. Ishitani, T. Murakami, S. Koizumi and T. Inuzuka, Appl. Phys. Lett., 57(5), 428 (1990).

5. M. Yoshikawa, H. Ishida, A. Ishitani, S. Koizumi and T. Inuzuka, Appl. Phys. Lett., 58(13), 1387 (1991).

6. B. R. Stoner and J. T. Glass, Appl. Phys. Lett., 60(6), 698 (1992).

7. S. Yugo, T. Kanai, T. Kimura and T. Muto, Appl. Phys. Lett., 58(10), 1036 (1991).

8. B. R. Stoner, B. E. Williams, S. D. Wolter, K. Nishimura and J. T. Glass, J. Mater. Res., 7(2), 1 (1991).

9. B. R. Stoner, G.-H. M. Ma, S. D. Wolter and J. T. Glass, Phys. Rev. B, 45(19), 11067 (1992).

10. B. E. Williams and J. T. Glass, J. Mater. Res., 4(2), 373 (1989).

11. D. G. Jeng, H. S. Tuan, R. F. Salat and G. J. Fricano, Applied Physics Letters, 67(10), (1990).

12. W. Zhu, B. R. Stoner, G. H. M. Ma, H. S. Kong, M. W. H. Braun and J. T. Glass, Phys. Rev. B, submitted (1992).

To be submitted to Phys. Rev. B

III. Photoluminescence and Raman Microscopy of CVD Diamond Defects from Nucleation to Formation of Continuous Films

L. Bergman, B.R. Stoner, K.F. Turner, J.T. Glass, and R.J. Nemanich

Department of Physics and Department of Materials Science and Engineering

North Carolina State University

Raleigh, NC 27695

Abstract

Photoluminescence and Raman spectroscopy are employed to explore the time-evolution of defect formation in CVD diamond films for stages of growth spanning nucleation to continuous film formation. Our research is concentrated on three types of defects which give rise to the 1.68 eV optical band, the sp^2 phase which exhibits a Raman feature center at 1500 cm^{-1} shift, and the broad-band luminescence at 565nm-800nm. The intensity of these features where correlated with the diamond Raman feature at 1332cm^{-1} to determine the relative dependence of the associated structures. Analysis of the 1332 cm^{-1} diamond feature showed two rates of diamond growth with a transition at the thickness where nearly complete coverage was obtained. The changes of the rates were attributed to the lowering degree of freedom available for the growth of the nuclei as well as to the formation of the sp^2 phase. The investigation of the different defects suggests the following conclusions: Si atoms are most likely responsible for the creation of the 1.68 eV optical centers which takes place at initial stages of growth, and structures associated with the broad luminescence and sp^2 bonding defects were not present in the isolated nuclei but were significantly present when a continuous film was formed.

I. Introduction

Investigation of defect formation in CVD diamond film is critical to understand the basic mechanisms of electronic transport and optical interactions which underlie applications in developing electronic and optical devices. In this study we employed Raman and photoluminescence microscopy (PL) to investigate the formation over time of defects in CVD diamond, from the very early stages of diamond nucleation through the formation of groups of particles and finally to the growth of continuous thick films. At each stage of the growth, the morphology of the sample was obtained from scanning electron microscope (SEM) images and this information was correlated to the PL and to the Raman line intensities of the defects. In this paper we present an analysis of the creation of three types of defects associated with optical bands at the 1.68 eV, the sp^2, and the broad-band luminescence at 565-800nm, for stages of growth spanning nucleation to continuous film formation.

One part of our experiment examined the 1.68 eV defect center, for which conflicting models have been proposed. Previous work has suggested a relation of the 1.68 eV center to the GR1 optical active center which exists in natural and synthetic diamond. Upon interaction with light the GR1 gives rise to the photoluminescence band at 1.673 eV. The GR1 defect center can be produced in any type of natural or synthetic diamond by the introduction of radiation damage into the diamond [1-4] which creates vacancies and interstitials of carbon atoms. It is commonly accepted that the GR1 band is associated with the natural vacancy center which possesses tetrahedral symmetry [5] and has an unpolarized zero-phonon line emission of 1.673 eV arising from a transition between the T_2 and the E state [6].

In many thin diamond films grown from the vapor phase, PL emission line can be observed at 1.68 eV which is a shift of 7-meV from the GR1 peak of the natural diamond. This shift may indicate that the 1.68 eV center originates from a different defect center than the natural vacancy. Various works show evidence that introduction of Si during growth increases the 1.68 eV peak significantly [7,8]. One explanation was that the Si atoms were incorporated into the diamond octrahedral lattice sites and formed a radiative center there [7]. Another study on Si-

implanted natural diamond showed that the 1.68 eV center was due to defects containing two interstitial silicon atoms [9]. Yet another possible explanation for the 7 meV shift is that it arises from the presence of the internal stress which exists in the individual crystallites of the CVD diamond films. This residual stress can induce the 6 to 7 meV shift of the GR1 center.

Another part of our experiment examined the broad-band luminescence. The broad luminescence band, extending from approximately 565 nm to 800 nm and centered at around 608 nm, has been observed in various luminescence studies. The broad band is exhibited in both cathodoluminescence (CL) spectra of natural and polycrystalline diamond [10-15,16], and has been also observed in the PL spectra of other studies [15-17]. In most of the PL and CL spectra, the 2.15 eV center was detected as well. This center has been attributed to the zero-phonon line (ZPL) of the interstitial nitrogen-vacancy complex. Some work suggests that the broad luminescence band is the result of vibronic interaction corresponding to the 2.15 eV ZPL [13]. Inspection of the PL spectra of hydrogenated amorphous carbon [18-19] reveals that a broad-band luminescence exists with similar characteristics as the diamond broad-band PL/CL. However, since the CVD diamond film was found to possess sp^2 amorphous-like carbon bonding, we surmise that the broad-band luminescence may be due to that type of defect.

In this paper we present our experiments and analysis of the formation of 1.68 eV, sp^2, and broad-band luminescence defects. Section A of this paper describes our measurements of the Raman line-width as well as the sp^2/sp^3 ratio and the absolute integrated diamond Raman line intensities as a function of the growth time. We found that at the very early stages of the deposition when the morphology of the substrate consisted of isolated diamond particles, no sp^2 phase was found and the Raman line-width exhibited a decrease with time. Furthermore the integrated diamond line followed a power-law increase with time. At later stages when coalescing of particles took place, sp^2 type bonding was found to form linearly with deposition time and the diamond line-width increased monotonically with time. Also, the integrated diamond line still exhibited power-law increase but with a smaller exponent than at early stages of growth. From our analysis of Raman line-width and diamond intensity, a common critical threshold time was obtained which

separated the early growth time phenomena from the longer time events, identical to the time when the diamond particles just started to cluster as observed in the SEM images.

Section B of this paper reports our study of the 1.68 eV defect center. In our research the PL measurements indicated that the formation of the 1.68 eV centers takes place at very early stages of nucleation and growth of the diamond particles. The rate of incorporation of the defects into the growing film diminishes as the sample becomes continuous. We also hypothesized that that plasma etching of the Si substrate is a possible mechanism to provide Si atoms which enhance the formation of the 1.68 eV optical centers. Our hypothesis about the interaction of plasma and Si substrate was checked via an experiment in which five diamond films were grown in different distances from the plasma. The 1.68 eV relative intensities of these samples were significantly higher for the samples which were placed next to the plasma core than for the samples which were located farther away.

In Section C we give the preliminary results of our study on the broad-band luminescence. The initial analysis of our work on broad-band luminescence indicates that the type of defects responsible for the broad PL does not exist in the isolated diamond nuclei, but rather tend to be created in later stages of growth. The broad PL follows similar growth-vs-time behavior as the sp^2 phase and therefore there is a possibility that the amorphous sp^2 bonding contributes to the broad PL in the CVD diamond film.

II. Experimental

Diamond samples for this study were grown in an ASTeX stainless steel microwave plasma CVD chamber described in detail in previous publications [20,21]. Briefly, the chamber consists of a cylindrical stainless steel cavity with an inner diameter of 6 inches. The plasma forms in a stable position at the center of the cavity and the substrate may be positioned relative to the plasma up to 8 cm downstream. The Si (100) substrates in this study were prepared by first abrading them with 1 μm diamond paste in order to increase nucleation density of the diamond

particles. The abrasion was followed by an ultrasonic cleaning in TCE, acetone, and methanol, a rinse with DI water and then drying with nitrogen.

For the study of defect formation as a function of time, a series of stop-growths was performed. The growth sequence was interrupted after deposition times of 1.5, 3, 5, 7, 10, 17 and 40 hours. Each step of the growth was followed by SEM, Raman microscopy, and photoluminescence analysis. Following the analysis, the sample was solvent-cleaned as discussed above and then reinserted into the growth chamber. The sample was grown in immersed mode and was located 0.5 cm into the plasma. The plasma consisted of 1% CH_4 in H_2 at 1000 sccm total flow. The plasma power, chamber pressure, and substrate temperature were maintained at 800 Watts, 25 Torr and 750° C respectively. For the study of the role of plasma in defect creation, five diamond samples were grown on Si substrates at positions 0, 1, 2, 3, and 4 cm below the plasma edge.

The photoluminescence and microwave Raman spectroscopy were carried out at room temperature using the ISA U-1000 scanning monochrometer. The samples were excited with the 514.5 nanometer line of an Argon-ion laser, which was focused on the sample to a spot of about 5 micrometer diameter. Focusing was facilitated by using the Olympus BH-2 microscope. The laser power at the sample was measured to be about 20 mW. The Raman spectra was taken at the region 1000-1800 cm^{-1} and the PL spectra was taken at the region 400-7000 cm^{-1} (2.36 - 1.54 eV). In order to check the spatial variation and to improve statistical significance the Raman and the PL data were taken at 12 different locations on the sample for each stage of the experiment. The data reported in this paper represent an average of these 12 points.

III. Results and Discussion

A. Analysis of the diamond and the graphitic Raman spectra

The first part of our experiment focused on an analysis of the Raman spectra as a function of growth time. In the Raman spectra of our cyclic growth sample, we observed two main Raman features centered at 1332 and at 1500 cm^{-1}. The Raman scattering at 1332 cm^{-1} has proved to be

an indication of sp^3 diamond bonding while the broad feature at 1500 cm^{-1} has been attributed to sp^2 amorphous-type graphitic bonding [22].

We first analyzed the diamond Raman line-width (FWHM) as a function of deposition time. Figure 1 shows the FWHM plotted as a function of growth time. The line-width exhibits a minimum at about 8 hours and a monotonic increase thereafter. The relatively large line-width at 1.5 hours and 3 hours of growth time may be attributed to the grain-size broadening mechanism of the small nuclei [23] as well as to the incorporation of the relatively large Si atoms into the diamond matrix which takes place at early stages as will be discussed in Section B of this paper. The minimum Raman line-width occurs at around 8 hours when the diamond particles are large (about 1.5 microns), and for the most part are isolated and just beginning to cluster as indicated by the SEM images shown in Figure 2. The broadening of the line-width at the later stages of deposition when the particles coalesce and continuous film forms can be attributed to three possible broadening mechanisms: the inhomogeneous strain induced by the increasing concentration of the grain boundaries in the film, the increasing presence of the sp^2-type defects, and the size effect of the secondary nucleation.

We next analyzed the diamond Raman integrated intensity as well as the sp^2/sp^3 ratio as a function of deposition time. Figure 4 shows the Raman spectra at the seven stages of growth time. The sp^2 feature at 1500 cm^{-1} starts to be noticeable at around 7 to 10 hours of growth time and becomes relatively large thereafter. For growth times under 7 hours the sp^2 feature was hard to detect in the spectra. Figure 3 shows for the same Raman spectra the plot of sp^2/sp^3 ratio versus growth time. The plot indicates the absence of sp^2 defects until around 7 hours and a linear increase for longer growth times.

The growth rate of CVD diamond is controlled by a complex dynamic balancing of the competitive growth of sp^2 and sp^3 phases and the preferential etching of sp^2 by atomic hydrogen [24,25]. Determination of the growth mechanism and the kinetics of the CVD diamond is beyond the scope of this research, but we do have several tentative conclusions based on our data which we now present.

The absence of sp^2-type defects at 1.5, 3, 5 and 7 hours of growth time, at which stages the morphology was observed to be one of unconnected nuclei of random orientation, may be the result of the preferential etching of the defects by the atomic hydrogen. Kobashi et al. [25] has found that the chemical reaction rate of graphite with hydrogen is about 30 times faster than that of diamond. Therefore, sp^2-type clusters are removed rapidly from the substrate surface and only diamond grains remain and grow. If this is the main mechanism preventing the presence of sp^2 at early stages, then we may conclude that the rate of sp^2 growth is about equal to the rate of its removal.

At later stages when coalescing and clustering of the nuclei occur resulting in formation of grain boundaries, the sp^2 phase follows a linear increase with deposition time. This implies that the rate of growth of sp^2-type defects is higher than the rate of its etching by the atomic hydrogen. One possible mechanism for the change in rate which takes place at around 8 hours is the incipient formation at that time of grain boundaries and grain edges where particles join. The grain boundaries and grain edges may provide favorable sites for the sp^2 phase to nucleate and grow. The hypothesis that sp^2-type bonding is present predominantly at grain boundaries and edges was also stated in the work of other groups [26,27].

In order to check how the diamond growth rate is impacted by the initial appearance of the sp^2-type defect and the morphology transition from isolated nuclei to clusters, we calculated the integrated intensity of the diamond Raman peak versus time. Figure 5 shows the plot of the diamond integrated intensity as a function of growth time. The plot indicates two different power-law growth rates of the diamond, and a transition time at around 8 hours. This transition time is consistent with the time of the initial appearance of the sp^2 defect and the time when a change in the morphology takes place.

The higher of the two growth rates occurs at early stages when the nuclei are purely diamond and in complete isolation from one another. Space is available for the grains to grow in both lateral and vertical directions. Above the transition time the growth rate is lowered due to the

coalescing which reduces the lateral degree of freedom available for the growth of the nuclei, as well as due to the competitive formation of the sp^2 phase in the growing film.

B. The 1.68 eV optical center

In the second part of our experiment the formation of the 1.68 eV centers as a function of growth time was examined. Figure 6 shows the spectra of the 1.68 eV band at 7 hours of growth time. For the cyclic growth sample, the PL integrated intensity of the 1.68 eV line was calculated and normalized to the diamond integrated Raman line for various growth times. The results shown in Figure 7 indicate an initial increase of the 1.68 eV relative intensity until a maximum is reached at about 8 hours; thereafter the PL relative line is seen to decrease with increasing growth time. The SEM images of this sample shown in Figure 2 reveal that initially the film consists of isolated diamond particles; after ~8 hours the diamond particles start to coalesce, forming grain boundaries until most of the Si substrate is covered by the growth.

A possible mechanism for the effect shown in Figure 7 is that etching of the Si substrate by the plasma releases Si atoms in the gas phase and redeposits them onto the growing diamond film. At early stages when the nucleation and growth of the isolated particles take place, the probability of creating the 1.68 eV centers is high since the Si substrate is almost entirely exposed. As the diamond nuclei continue to grow in an isolated fashion, the concentration of the defect centers increases. At deposition times longer than 8 to 10 hours, less of the Si substrate is exposed to the plasma, resulting in reduced concentration of the 1.68 eV defect centers.

The absolute integrated intensity of the 1.68 eV line was also measured at ten different positions on the ten-hour growth sample. No significant variation in intensity was found which implies that the final spatial distribution of these defects was nearly uniform across the sample. For the sample of forty-hour growth time, large fluctuations in the 1.68 eV absolute intensities were observed across the sample. Furthermore, on the average the PL intensity was 35% lower than the absolute integrated intensity exhibited by the ten-hour sample which possessed the maximum concentration of defects. The diamond Raman signal also exhibited up to 30% variation

in intensity across the sample. The above observations suggest that the film thickness and the presence of grain boundaries caused the luminescence of the forty-hour sample to scatter, thereby making the PL signal hard to collect. This scattering of the luminescence implies that the 1.68 eV centers reside mainly next to the interface of the diamond and the Si substrate, and that less of the defects are present in the bulk of the diamond film.

To support the assumption that plasma interaction with Si substrate initiates formation of the optical defect centers, five incomplete diamond films were grown at different distances from the hydrogen plasma. Figure 8 shows the resulting 1.68 eV integrated relative intensity as a function of distance from the plasma, and indicates that the film which was grown immersed in the plasma exhibited the highest concentration of the 1.68 eV centers. The film which was grown four cm from the plasma exhibited very small concentrations of these centers. Saito et al. [28] have found other evidence of hydrogen plasma interaction with the Si substrate: their experiments revealed that when placing the Si substrate in the plasma center, etching and redeposition of Si atoms was the predominant reaction due to the high concentration of electrons and hydrogen radicals.

C. The broad-band PL at 565nm - 800nm

In this section we present an analysis of the broad-band photoluminescence as a function of growth time. Figure 9 shows the broad-band PL spectra for the isolated diamond nuclei at 3 hours of growth time and for the continuous film at 40 hours. The spectra of the continuous film exhibits a strong PL band ranging from approximately 1000 cm^{-1} to 6000 cm^{-1} (565nm - 800nm), and centered at around 2 eV (~3000 cm^{-1}). The broad-band PL is not present in the spectra of the isolated diamond nuclei.

The graph of the relative integrated intensity of the PL band versus growth time is shown in Figure 10. The PL band was not observed in the spectra of the initial stages of growth, and was noticeable only from 7 to 40 hours during which interval it behaved linearly with growth time. The time-evolution of the broad-band PL is similar to that of the sp^2-type bonding (see Figure 3). The similarity in the formation of the two types of defects may be an indication that the presence of

defects which caused the broad PL is due to the sp^2 carbon bonding which exists in disordered configuration in the diamond film.

Broad band PL spectra very similar to those found in our work have been observed in many studies of amorphous hydrogenated carbon material (a-C:H) which possess a random network of sp^2 and sp^3 bonding configuration [18-19]. The line-shape and the peak position of the PL was found in these studies to vary from sample to sample depending on the growth condition. The broad PL in a-c:H has been assumed to originate from transitions in the exponential distribution of tail states which extend into the forbidden gap. The presence of tail states is a consequence of the lost long-range order in the material.

Other studies using cathodoluminescence (CL) spectroscopy suggest that the broad luminescence in diamond is due to interaction of the 2.16 eV ZPL center with the lattice vibration (vibronic interaction) [10,12-14]. The 2.16eV band which arises from the interstitial nitrogen-vacancy complex was observed in our spectra and had very weak intensity. The nitrogen in our diamond film was probably deposited from the residual amount of this element which existed in the environment of the growth chamber.

The fact that both PL and CL extend over the same range of luminescence and have similar line-shape does not exclude the possibility that CL is due to a different type of defect center than that of PL, since the two spectroscopies differ in their energy range and in their cross-section. The determination of the origin of the broad luminescence will be addressed in a future study.

From our present data we conclude that the type of defect responsible for the broad-band PL in the CVD diamond does not form at early stages when isolated nuclei constitute the morphology. The defects instead start to form at approximately 7 hours of growth time and have increasing concentration thereafter. A possible type defect which may cause the broad PL is the amorphous sp^2-type bonding which has time-evolution consistent with the PL luminescence intensity.

IV. Conclusions

Our research suggests the following conclusions about the formation of defects in the CVD diamond:

1. The diamond line-width exhibits an optimum when the particles are large and disconnected. As the film became continuous, a broadening of the line was observed, and was attributed to the strain induced by the grain boundary and to the sp^2 phase both which appear at later stages of the growth.

2. The Raman spectra revealed that the isolated nuclei did not contain sp^2-type defects. At later stages when clustering occurred and grain boundaries formed, sp^2 phase was found to increase with growth time. The increase of the sp^2 defect concentration may be attributed to the presence of the grain boundaries which provide sites for the sp^2 type bonding.

3. From an analysis of the integrated diamond Raman line as a function of time, a characteristic time was obtained for which a morphological transition of isolated nuclei to clusters took place. The characteristic time marked also the time when the sp^2 phase started to appear. We surmise that These two events were responsible for the decreased growth rate of the diamond.

4. The 1.68 eV defects are found to be created mostly at early stages of diamond nucleation and growth when most of the substrate is exposed to the plasma. Hence higher concentrations of this type of defect reside in the vicinity of the Si substrate and less in the bulk of the diamond film. In our experiment, no variation in concentration of the 1.68 eV defect was found across the sample.

5. The plasma interaction with the Si substrate is essential to the formation of the 1.68 eV defect in the CVD diamond. Since the creation of the optical center is greatly enhanced by the availability of Si, most likely the center contains Si atoms. This conclusion is supported by our observations that the relative integrated intensity of the 1.68 eV band of the samples which were grown in various distances from the plasma exhibited a decrease with distance from the plasma, combined with the

finding that the creation of the defects took place at early stages when most of the Si substrate was exposed to the plasma.

6. The broad PL band which centers at ~2eV was not observed in the spectra of the early stages of nucleation and growth, but was present in the spectra of the later stages. The broad PL and the sp^2 intensities both follow similar time evolution. Amorphous carbon hydrogenated material, which contains the same bond configuration as the sp^2 phase in the diamond film [18-19], exhibits broad photoluminescence spectra similar to that observed in our spectra. These two observations lead us to suggest that the sp^2 bonding configuration may give rise to the broad-band luminescence. This topic will be investigated in a future study.

In summary, the isolated diamond nuclei contain only the 1.68 eV optical defect. The diamond bulk film contains the sp^2-type defects and the defects which give rise to the broad PL.

References

1. C.D. Clark and J. Walker, Proc. Roy. Soc. London A,234 (1973).
2. C.D. Clark and E.W.J. Mitchell, in: *Proc. 1970 Conf. Radiation Damage in Semiconductors,* edited by J.W. Corbett and G.D. Watkins (Gordon and Breach, London, 1971) p.257.
3. A.M. Stoneham , *Theory of defects in solids* (Clarendon Press, Oxford, 1975).
4. J. Walker, Rep. Prog. Phys.**42**, 1605 (1979).
5. G. Davis, in: *Chemistry and physics of carbon* **13**, edited by P.L. Walker and P.A. Thrower (1977), p.2.
6. C.D. Clark and C.A. Norris, J. Physics C: Solid State Phys. **4**, 2223 (1971).
7. A.R. Badzian, T. Badzian, R. Roy, R. Messier, and K.E. Spear, Mat. Res. Bull. **23**, 531 (1988).
8. J. Ruan, W.J. Choyke and W.D. Partlow, Appl. Phys. Lett. **58**, (1991).
9. V.S. Vavilov, A.A. Gippius, A.M. Zaitsev, B.V. Deryagin, B.V. Spitsyn and A.E. ALeksenko, Sov. Phys. Semicond. **14**, 1078 (1980).
10. G. Davies, J. Phys. C: Solid State Phys. **12**, 2551 (1979).
11. R.J. Graham and K.V. Ravi, Appl. Phys. Lett. **60**, 1310 (1992).
12. A.T. Collins and S.H. Robertson, J. Mater. Sci. Lett. **4**, 681 (1985).
13. L.H. Robins, L.P.Cook, E.N. Farabaugh, and A. Feldman, Phys. Rev. B **39**, 39 (1989).
14. A.M. Zitsev, A.A. Gippius, and V.S. Vavilov, Sov.Phys.Semicond. **16**, 252 (1982).
15. E.S. Etz and E.N. Farabaugh, A. Feldman and L.H.Robins, *SPIE Vol. 969 Diamond Optics*, 86 (1988).
16. J.A. Freitas, Jr., J.E. Butler and U.Strom, J. Mater. Res. **5**, 2502 (1990).
17. D.S. Knight and W.B. White, *SPIE Vol. 1055 Raman Scattering, Luminescence, and Spectroscopic Instrumentation in Technology,* 144 (1989).
18. S. Lin, and B.J. Feldman, Phys. Rev. Lett. **48**, 829 (1982).
19. J. Wagner and P. Lautenschlager, J. Appl. Phys. **59**, 2044 (1986).

20. B.R. Stoner, J.T. Glass, L. Bergman, R.J. Nemanich, L.D. Zoltan, and J.W. Vandersande, J. Electron. Mat. **21**, 629 (1992).

21. B.R. Stoner, G.-H.M. Ma, S.D. Wolter, and J.T. Glass, Phys. Rev. B **45**, in press (1992).

22. R.J. Nemanich, J.T. Glass, G. Lucovsky, and R.E. Shroder, J.Vac.Sci. Technol. A **6**, 1783 (1988).

23. Y.M. LeGrice, R.J. Nemanich, J.T. Glass, Y.H. Lee, R.A. Rudder, and R.J. Markumas, *Mat. Res. Soc. Symp. Proc. Vol. 162*, 219 (1990).

24. A.R. Badzian, R.C. DeVries, Mat. Res. Bull. **23**, 385 (1988).

25. K. Kobashi, K. Nishimura, Y. Kawate, and T. Horiuchi, Phys. Rev. B **38**, 4067 (1988).

26. Y. Sato and M. Kamo, Surface and Coatings Technology **39/40**, 183 (1989).

27. A.V. Hetherington, C.J.H. Wort, and P. Southworth, J. Mater. Res. **5**, 1591 (1990).

28. Y. Saito, S. Matsuda, and S. Nogita, J. Mat. Sci. Lett. **5**, 565 (1986).

Figure Captions

Figure 1. The diamond Raman line-width (FWHM) as a function of deposition time. The optimum of the line-width occurs at ~8 hours.

Figure 2. The SEM micrographs of the diamond sample at 1.5, 3, 10 and 40 hours of deposition time.

Figure 3. The relative Raman intensity of the sp^2 type bonding versus growth time. The graphitic component is not present in the spectra at the early stages of growth (1.5 ~ 7 hr.).

Figure 4. The Raman spectra at the seven stages of deposition time: 1.5, 3, 5, 7, 10, 17 and 40 hours.

Figure 5. The integrated intensity of the diamond Raman peak as a function of growth time. The transition from higher to lower growth rate occurs at ~ 8 hr.

Figure 6. The PL and Raman spectra of the diamond particles at 7 hours of growth time.

Figure 7. The relative integrated PL intensity of the 1.68 eV band as a function of deposition time. The highest intensity occurs at ~7 hours.

Figure 8. The relative integrated PL intensity of the 1.68 eV band versus distance from the plasma during growth.

Figure 9. The broad PL spectra of (a) the isolated nuclei at 3 hours and (b) of the continuous film at 40 hours of growth time.

Figure 10. The relative integrated intensity of the broad band PL versus deposition time. The broad band is not present in the spectra at the early stages of growth.

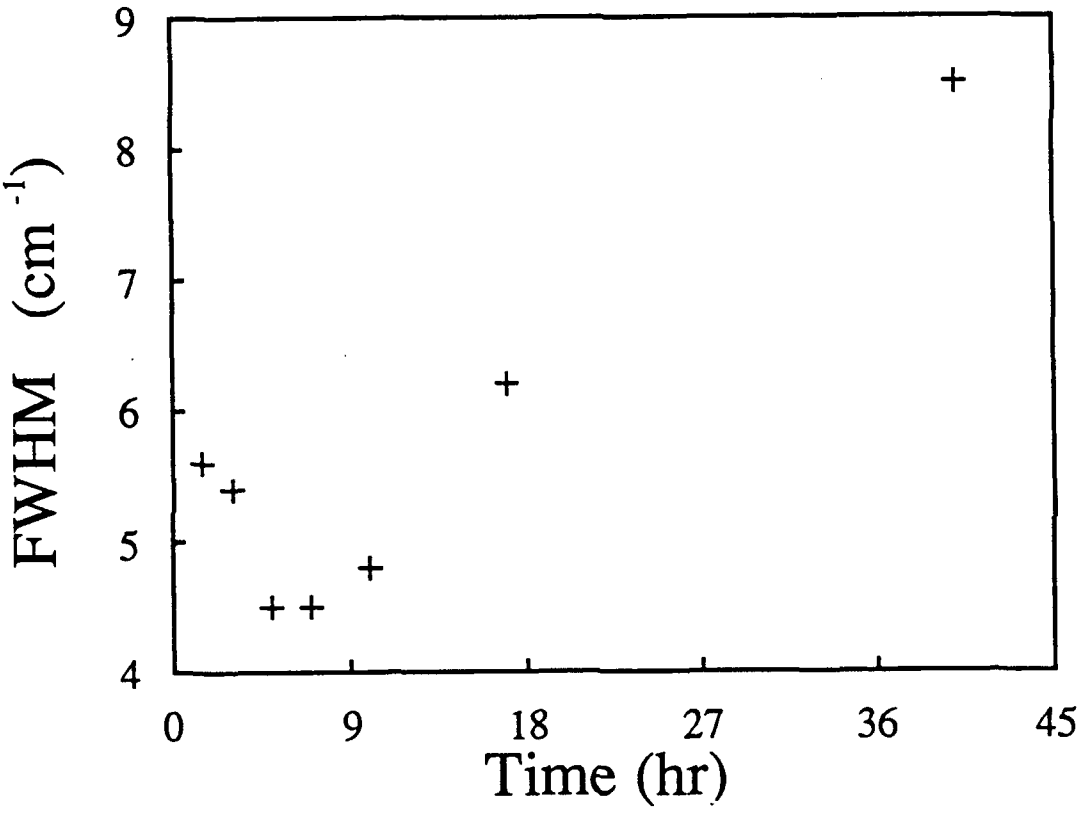

Figure 1


WD17
BS74A0 15.0kV X10.0K 3.00µm

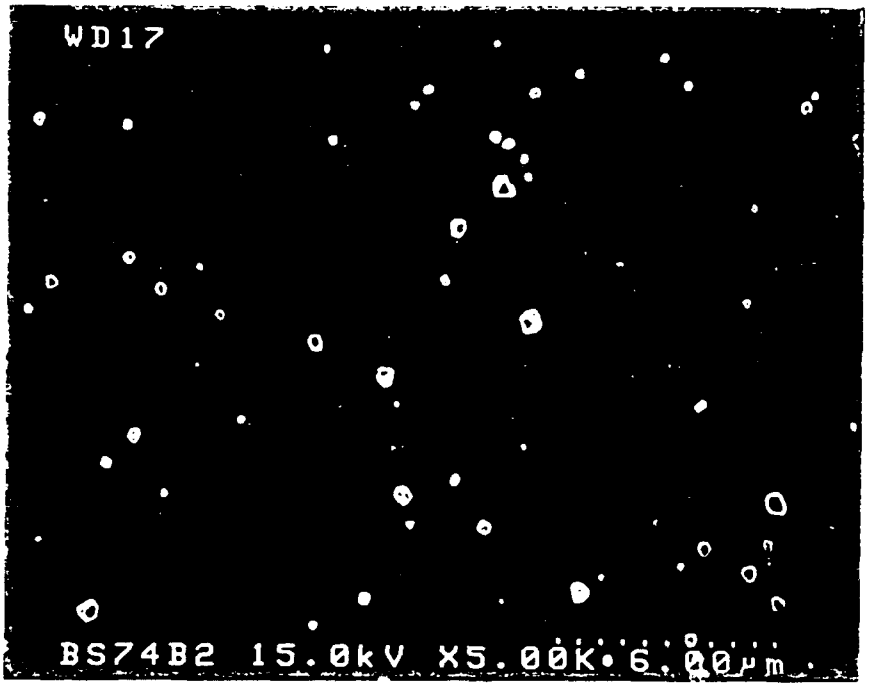
WD17
BS74B2 15.0kV X5.00K 6.00µm

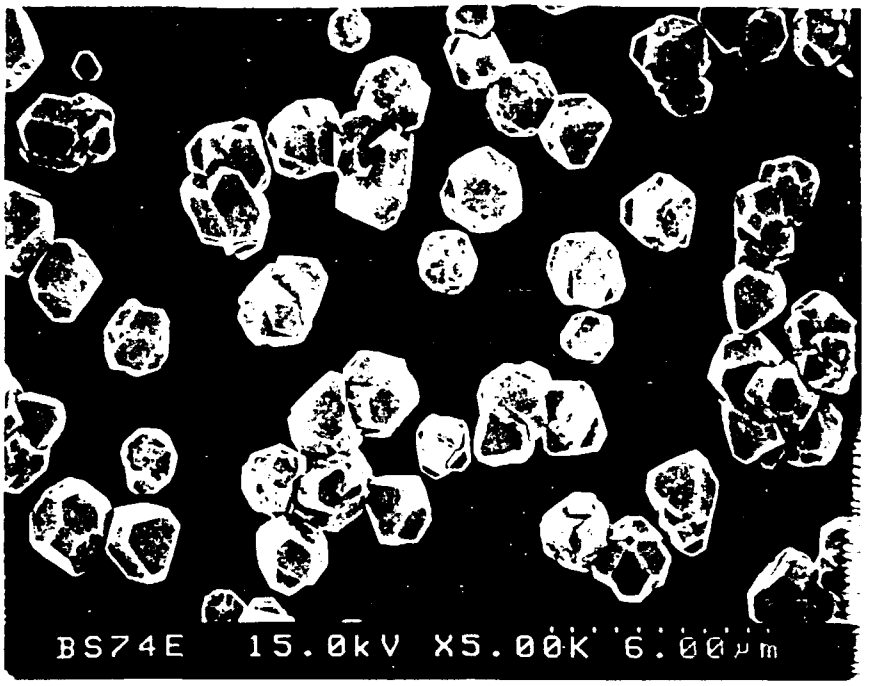
BS74E 15.0kV X5.00K 6.00µm


BS74HB 25.0kV X5.00K 6.00µm

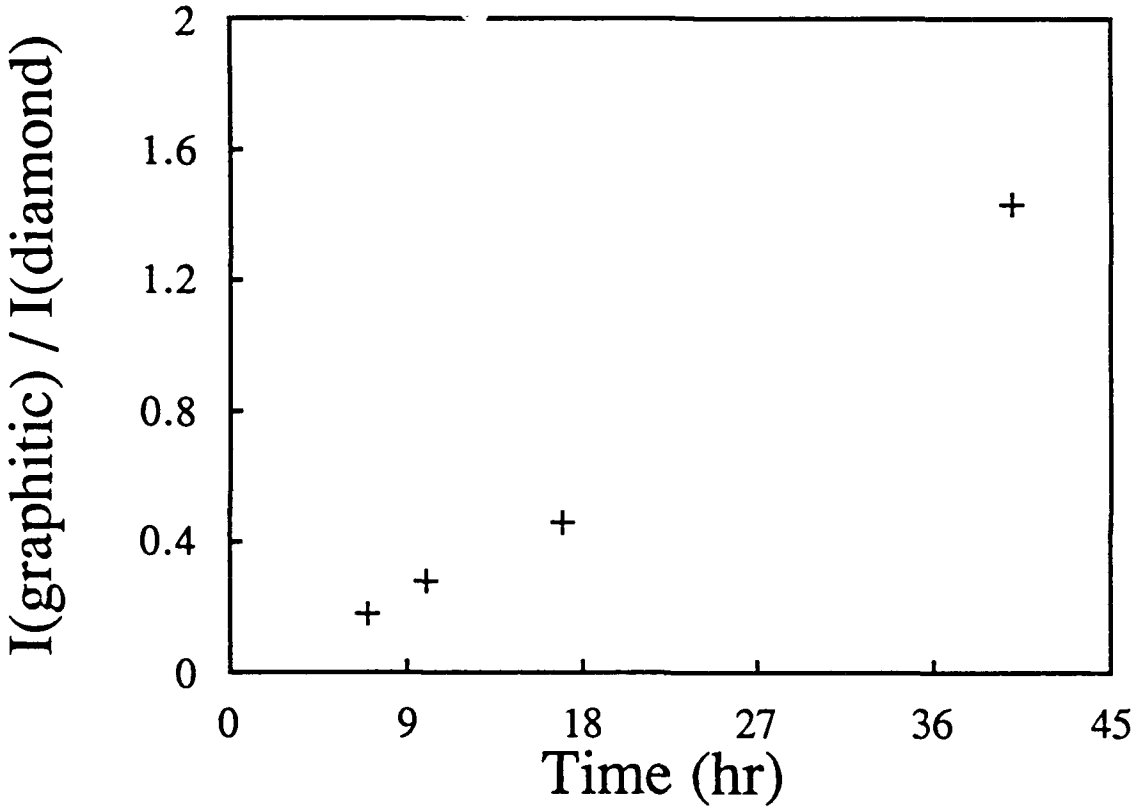

Figure 3

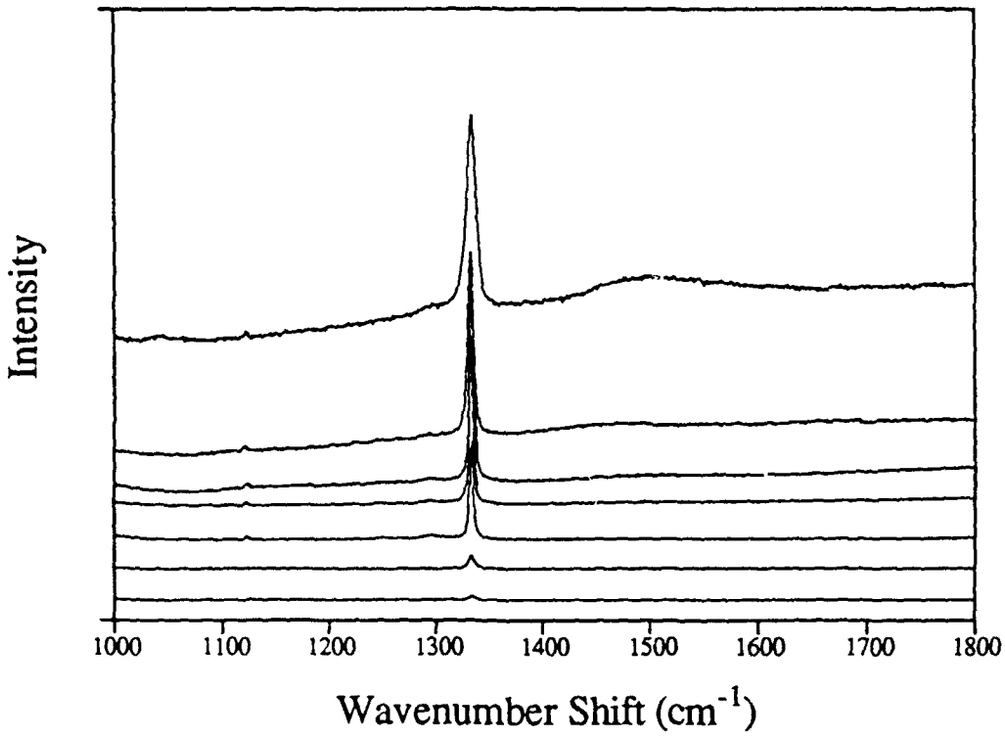
Intensity
1000
1100
1200
1300
1400
1500
1600
1700
1800
Wavenumber Shift (cm-1)

Figure 4

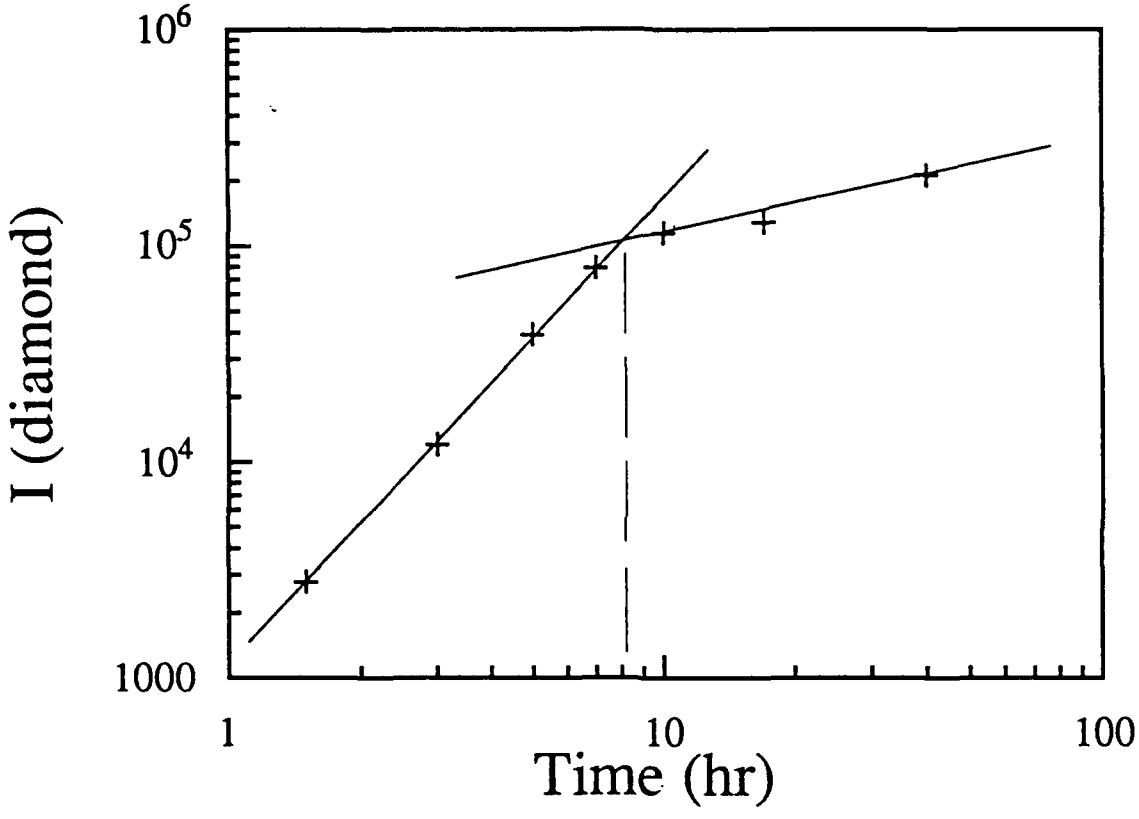

Figure 5

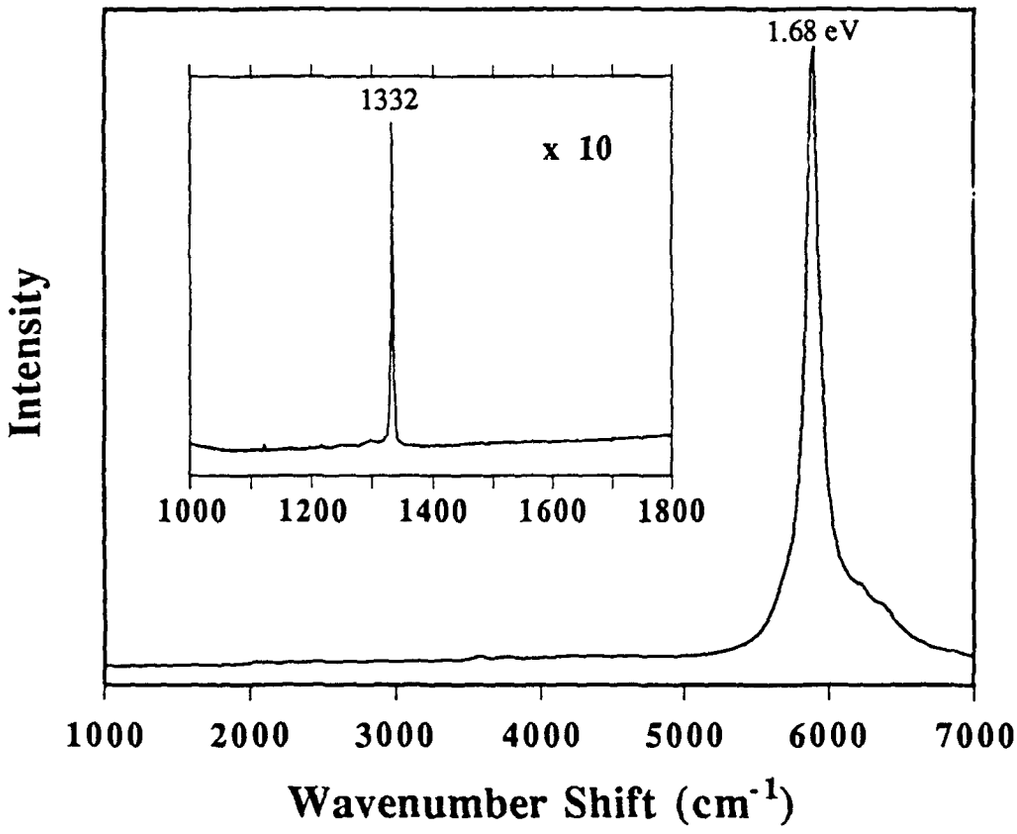
1.68 eV
1332
x 10
Intensity
1000
1200
1400
1600
1800
1000
2000
3000
4000
5000
6000
7000
Wavenumber Shift (cm-1)

Figure 6

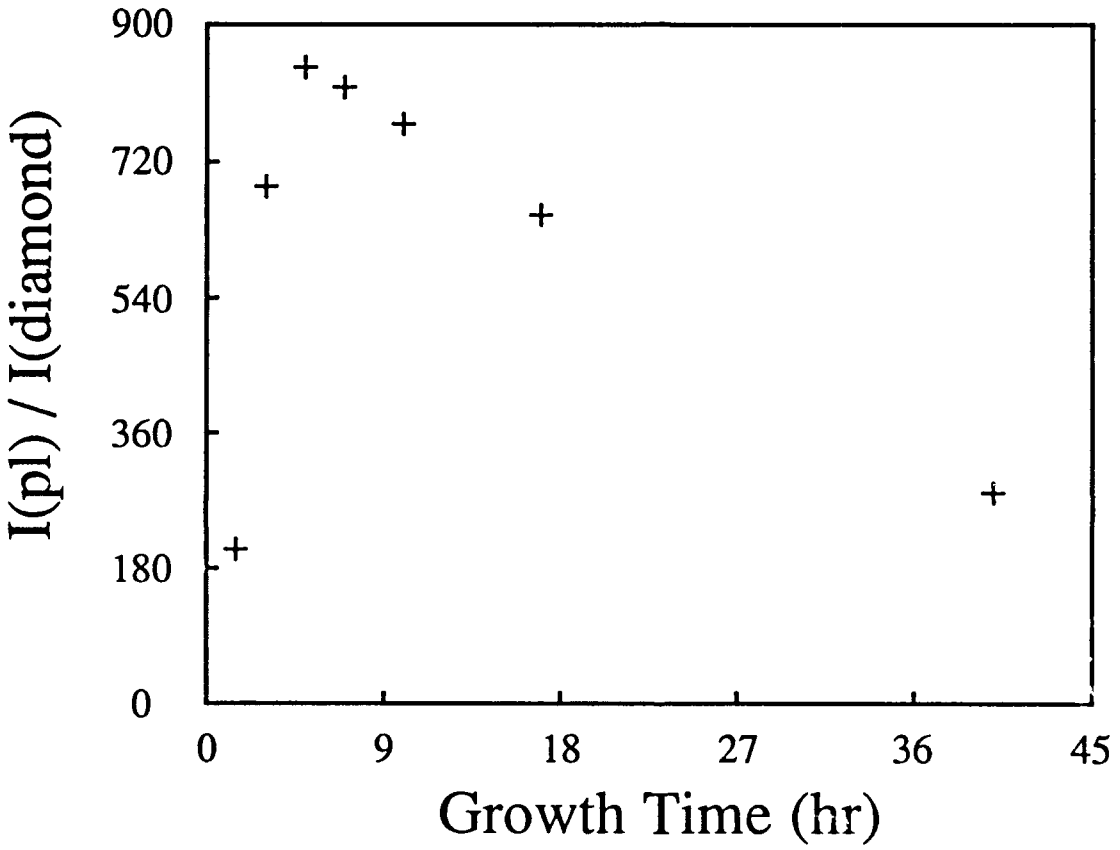

Figure 7

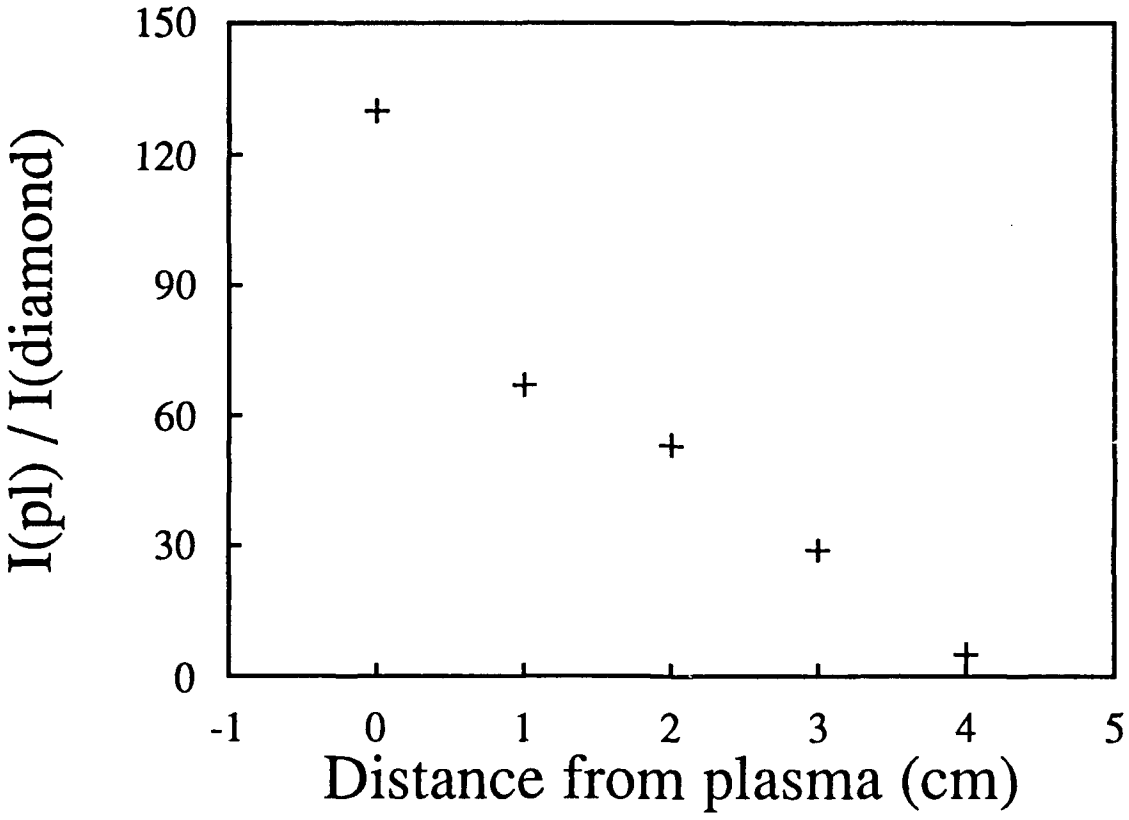
150
120
90
60
30
0
I(pl) / I(diamond)
-1
0
1
2
3
4
5
Distance from plasma (cm)

Figure 8

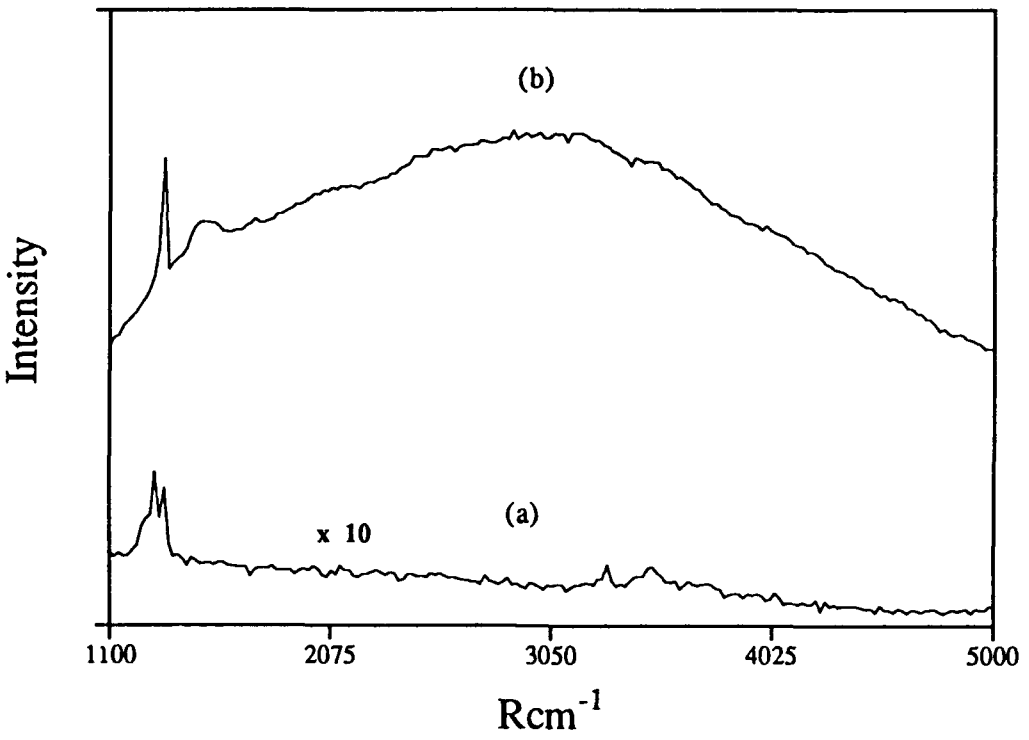

Figure 9

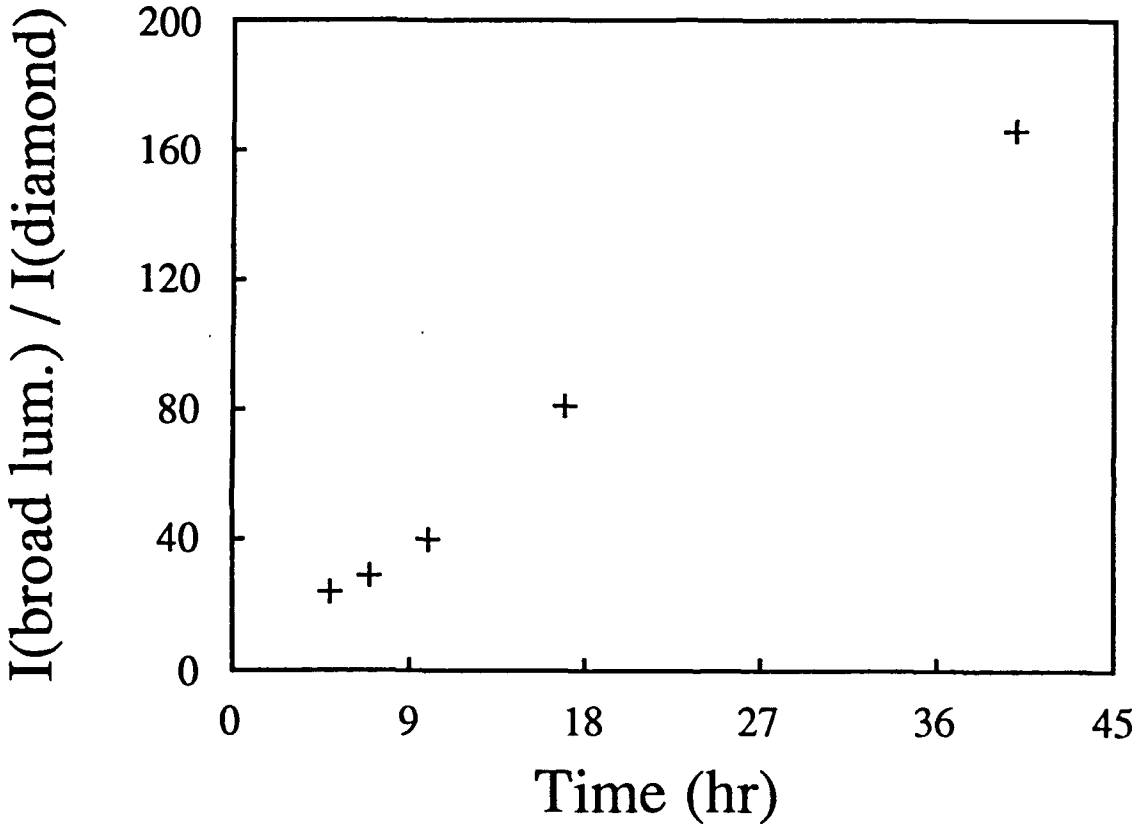

Figure 10

To be submitted: J. Appl. Phys.

IV. Characterization of the Electronic Properties of Diamond Film Growth by Scanning Tunneling Spectroscopy

K.F. Turner and R.J. Nemanich

Department of Physics and Department of Materials Science and Engineering

North Carolina State University

Raleigh, NC 27695-8202

Abstract

The growth of CVD diamond films on silicon and germanium has been studied by scanning tunneling spectroscopy (STS). STS allows for the characterization of the surface electronic states. Since the technique is utilized with scanning tunneling microscopy, changes in current voltage characteristics can be spatially resolved on an sub-micron scale. Substrates of silicon, β-silicon carbide, and single crystal C(100) were cleaned and examined by STS in air to provide examples of their electronic structures imaged in the ambient. The electronic structure of the carbonaceous films which form on the Si substrates prior to and during nucleation were characterized, and both doped and undoped diamond nuclei formed on Si were compared. While the bulk electronic structures were found to be similar, the surface electronic structures differed significantly. The surface of a continuous polycrystalline diamond film showed electronic structure similar to that of single crystal diamond. The Si substrate interface was studied on a "free-standing" film prepared by etch removal of the Si. The etched and growth sides of this film showed different electronic structures. The growth surface had a structure similar to that of the crystalline diamond while the etched side showed evidence of β-silicon carbide and graphite electronic structures.

I. Introduction

The possibility of growth of diamond thin films under conditions of low temperature and pressure was realized in the 1950's [1]. It has only been in the last twenty years that the process has become economically and technically feasible. More recently, the thrust of most of the diamond research has focused on the film quality and growth rates [2]. The surface chemistry involved is understood in the simplest terms [3], but the growth of high quality chemical vapor deposited (CVD) diamond has been achieved. Many different surface and bulk characterization methods have been applied to study the growth processes, nucleation, and the resulting complete diamond films [4-6].

A relatively new characterization process is scanning tunneling microscopy (STM) and its associated microscopies. One of the techniques related to STM, used to identify surface electronic structure, is scanning tunneling spectroscopy (STS). The utility of STS, where current-voltage data is taken at the same time that the STM image is recorded, was demonstrated by Hamers et. al. [7]. This concurrent measurement of topographical and electronic structures allows for the correlation of the two properties. The process has been used to characterize the electronic structures of many surfaces including silicon [8-10] and germanium [11-13]. Wide band gap semiconductors have been examined less, but examples of STS applied to SiC [14,15] and ZnO [15] surfaces have been reported. In the characterization of diamond nucleation and growth, some recent examples of scanning tunneling spectroscopy (STS) have been reported [16, 17].

The purpose of this study is to investigate the electronic structures of the doped and undoped diamond nuclei, the interface between diamond and silicon, and surfaces involved in the growth of diamond. The STS results discussed in this paper were obtained with the sample and STM in air. This limits the resolution of the process, but does not preclude its usefulness. STS measurements in air have, however, previously been used to delineate pn junctions [18] in Si and to identify defects in semiconductors [19], to name a few. As will be discussed more fully in the

discussion section, STS performed in the ambient is useful as long as the limits of the technique are understood.

II. Experiment

The STM analysis of the surface was carried out over a wide range of parameters. The analysis was performed using a Park Scientific Instruments STM-SA1, which is an ambient STM. The scans of the surface covered ranges between 100Å - 10mm. The tip was scanned at rates corresponding to between 0.08 to 2 Hz and tunneling currents ranging between 0.2nA to 4nA. The parameters of the system were changed for each sample in order to enhance imaging of that particular film or substrate.

STS results were obtained in the following manner. First, the surface was imaged by STM. Regions of interest were identified and these regions were scanned over ranges between 100Å - 200Å. STS was performed over this region to identify its uniformity. If the current-voltage curves were uniform, to within a level of noise, then STS was performed over the area for eight values of the set point current, i. e. eight different tip to sample distances. Several such regions were examined for each surface. The STS spectra presented here have been averaged over all eight curves taken at the eight values of the set point current. The STS curves were then smoothed to allow for better interpretation of the major peaks of each spectrum. All of the results presented in this work were obtained using etched or mechanically ground PtIr tips.

It has been shown that the ratio of the differential conductance (dI/dV) to the conductance gives a relative measure of the surface density of states [20, 21]. To analyze the data, derivatives of the current-voltage curves were calculated from the I-V curves. The derivatives were then divided by the conductance (I/V) to normalize the data.

One of the objectives of this work is to characterize the electronic structure of diamond nuclei. In order to accomplish this goal, many samples were needed to provide standards with which the results could be compared. The Si(100) substrate was cleaned with HF acid and

examined within 10 minutes with the STM. The graphite sample was cleaved with a piece of adhesive tape to produce a clean surface.

The undoped nucleation samples were prepared by microwave plasma CVD on 1 inch diameter Si(100) substrates. The substrates were polished with 0.25 mm diamond powder for 5 minutes and then solvent cleaned. The substrates were exposed to growth conditions for 1 hour for both doped and undoped studies. In both cases, the growth occurred at a pressure of 35 Torr, a methane to hydrogen ratio of 0.5% with a total flow rate of 1000 sccm and an average substrate temperature of 800°C. Doped diamond nuclei were also grown under the same conditions as above. For the doped nuclei, diborane was included in the gas mixture at a level of 10.0 ppm. SEM micrographs were obtained from the surfaces to provide an estimate of the nucleation density.

Complete diamond films grown on Si were prepared by hot filament CVD on Si<100> substrates. The substrates were preseeded with diamond powder, and the gas flow of 100 sccm hydrogen, 1.5 sccm methane, and 0.4 sccm oxygen were controlled to obtain diamond growth. The thickness of the film was between 1mm and 2 mm. Diborane was introduced into the gas flow to dope the sample. The film was doped with a gas phase concentration corresponding to 6 x 10^{19} per cm^3. The boron incorporation efficiency was determined to be approximately 20% by SIMS analysis.

The freestanding film used in the exploration of interfacial properties was originally grown on a Si<100> substrate. The substrate was polished with 0.25 mm diamond powder and then solvent cleaned. The sample was grown for 27 hours. The growth occurred at a pressure of 90 Torr, a methane to hydrogen ratio of 0.5% with a total flow rate of 100 sccm and an average substrate temperature of 900°C. Diborane was included in the gas mixture to dope the film and a doping concentration of 1020 atom/cm^3 was subsequently measured by SIMS. The silicon substrate was removed by chemically etching using a solution of nitric and hydrofluoric acid.

III. Results and Discussion

A. Electronic Structure of Single Crystal Diamond

When STS is performed under UHV conditions, the presence of surface absorbates can be eliminated, the atomic structure can be observed and a measure of the surface structure can be obtained. Without absorbates on the surface, all observed electronic structure must be ascribed to the electronic structure of the sample and the tip. Variations of the electronic structure can often be measured over the surface to an atomic scale. In some cases, STS can also be used for the determination of the presence of surface absorbates.

When STS is performed in air, the situation is more difficult. For most surfaces examined in the ambient, the presence of absorbed molecules is almost assured. It is, therefore, not likely that every peak can be attributed to the atomic scale electronic structure of the surface. It is, however, possible to identify significant features of the electronic structure. To that end, standards were developed for several surfaces imaged in air which can be compared with suitable results taken under UHV conditions. Using these standards, the electronic states of the growth surfaces can be identified.

The (dI/dV)/(I/V) curve, referred to as a surface DOS curve, of boron doped type IIb single crystal diamond is shown in Figure 1. A schematic of band structure of diamond and how it is measured by STS is shown in Figure 2. The point of zero bias voltage corresponds to the Fermi level position (E_F), indicated as E_i in Figure 2. For negative applied bias voltages, states with energy greater than E_F are probed, i. e. probing empty electronic states. For positive biases, the inverse is true. We assume that the PtIr tip has a metallic density of states and does not significantly influence the surface DOS curves. There is a region of low conductivity between -3.2eV and 1.0eV. This presumably is the surface bandgap of diamond. It is consistent with the p-type character of the sample, with an increase at 1.0eV below E_F due to tunneling from the valence band.

The authors also assert that the sudden rapid increase in the DOS beginning at -3.5eV is due to Fowler-Nordheim tunneling [22]. This sharp increase is observed, in some form or

another, for almost all of the diamond samples in this study. This effect has been observed by other authors conducting STM investigations of Si and Cu surfaces [23, 24]. It is observable at bias potentials for diamond because the conduction band edge is close to the vacuum level. In fact, for some surfaces of diamond, near the onset of tunneling into the conduction band, a small negative electron affinity has been observed [25,26]. We were not able to determine if the diamond surfaces exhibited a negative electron affinity, because the spectra presented here do not have a sufficient energy resolution. The energy resolution for all of the spectra taken over the ±6V range is 0.15eV. In principle, it would be possible to measure this effect by STS.

B. Electronic Structure of Diamond Nuclei

In order to effectively characterize the electronic structures of the surfaces of diamond nuclei, standards need to be established for STS performed in air. It is for that reason that the STS spectra are presented for silicon, graphite, silicon carbide, and doped polycrystalline diamond grown on silicon. These spectra can, in turn, be compared with spectra obtained under UHV conditions.

The spectrum shown in Figure 3 was obtained from a Si(100) surface which was cleaned with HF and examined immediately after. Previous studies have established that immediately after HF etching, the Si surface is terminated with hydrogen. Through examination of Figure 3, a region of low conductivity can be observed between -0.5eV and 0.4eV. This probably represents the surface bandgap of the Si(100). This value for the bandgap is somewhat smaller than expected, but is still consistent with results found under UHV conditions [27, 28]. Several prominent peaks can be observed at -1.9eV, -1.4eV, 0.9eV, and 2.5eV. While several of these peaks are close to the values obtained in UHV, correspondences between peaks found in the ambient and those found under UHV conditions cannot be assured.

The surface DOS spectrum of n-type Si terminated SiC is presented in Fig. 4. Here, the region of low conductivity runs from 0eV to 2.0eV. This feature probably corresponds to the surface bandgap. The Si terminated surface accumulated an oxide before examination by STM,

as evidenced by its poor imaging quality. This also can be inferred because of the differences between these results and those obtained under UHV conditions [14]. The most prominent features that we observe are the "shoulder" extending from 2.0eV to 3.4eV, the low conductivity region mentioned above, and a peak at -1.0eV.

The surface DOS spectrum for highly oriented pyrolithic graphite (HPOG) are shown in Fig. 5. Since HOPG does not readily oxidize, it is possible to identify actual bonding, antibonding, or surface states. In this case, the low conductivity regions extends between 0eV and 0.6eV. Peaks are located at +3.5eV, +1.5eV, -1.3eV, -1.7eV, -2.5eV, and -3.6eV. Comparing these results with the work of Fuchs et al. [29], and the calculations of Selloni and others [30], all of these peaks have been reported or predicted with the exception of the peak at +3.5eV. Selloni calculated that there is a state at +2.5eV and this state has been observed in other studies [30]. It is likely that the +2.5eV peak is present in the spectrum, but it is obscured by the presence of the peak at +3.5eV. The origin of the 3.5eV peak is unknown, but may be due to the presence of absorbates on the surface.

The surface DOS of a doped polycrystalline diamond film grown on silicon is shown in Figure 6. A region of low conductivity is shown between -2.2eV and 1.0eV. A peak is observed at +1.8eV, a shoulder extending from -2.5eV to -3.8 eV, and an increase in the current starting at 3.0eV. It is important to note that this gap is less than the 5.4eV expected for diamond. One rationale for this change is that the actual gap ends at +2.4eV, which can be found by tracing down the sharp increase at high positive bias. In that case, the peak at +1.8eV would most likely be due to the presence of surface states, a bulk impurity level, or surface contaminants.

The surface DOS spectrum for a small nucleus of undoped diamond deposited on Si are shown in Fig. 7. As described previously [31], examination of the undoped diamond nuclei by photoluminescence showed that the defect density in the nuclei was relatively large. We asserted that it was due to this large defect density that imaging of undoped nuclei by STM was possible. The surface DOS results support these results. The spectrum shows an electronic structure with a bandgap of 5.3 eV with endpoints of -2.0eV and 3.3eV. There appears to be several small peaks

within the gap that may be attributed to defect levels. Note also the increase in the surface DOS for high positive bias voltages, as in the spectrum shown in Figure 6, which was also grown on silicon.

From the same sample, Figure 8 shows the surface DOS from a region near a nucleus on the substrate. It has been proposed that carbonaceous [32] or silicon carbide [33] layers form on the surface prior to or during diamond deposition. It is useful to compare the spectrum in Figure 8 with that of Si (Figure 3). The peaks of the spectrum of the surface DOS, which are at -1.8 eV, -1.1eV, 1.0eV, 1.2eV and 1.5eV, do not align with those found in the spectrum of Si. We can conclude that a film has formed on the surface that has altered the electronic structure. A few of the peaks in Figure 8 are in the same positions as peaks in the STS spectrum of HOPG, but the general shapes of the two spectra are very different. The electronic structure does not closely resemble any of the standards presented in Figures 1-6. The characterization of the electronic structure of this growth surface may require more standards than have been examined in this study.

Examination of Figure 9, which provides a contrast of the electronic structure of the undoped nuclei with the electronic structure of the growth surface, may suggest an alternate interpretation. When molecules are absorbed on the surface, it has been shown that the molecules contribute discrete levels to the DOS if they are loosely bound to the surface [34]. Other studies [35] have shown that, depending on how the diamond reactor is shut down after growth, a layer of hydrocarbons may be left on the surface. If this interpretation is correct, then the spectrum shown in Figure 8 could show the surface DOS of a carbon layer with loosely bound absorbates on its surface.

The surface DOS for a doped nucleus grown on silicon is presented in Fig. 10. The most prominent feature is the peak at 3.5eV. If the slope of the line from 3.5eV to 2.2eV is extrapolated to the lowest DOS value, a region from 2.2eV to -2.1eV can be estimated to be the bandgap region. Two mid-gap states can be identified: one at +1.0eV and the other at -1.2ev.

The surface DOS from a region near a doped nucleus on the substrate is shown in Figure 11. Again, the peaks of this spectrum, at -0.8eV, 0.7eV, 1.0eV, 1.2 eV, and 1.5eV, do not seem to correspond to any peaks in the spectrum of silicon (Figure 3). Perhaps more surprisingly, all of the peaks at positive bias voltages, where filled states are being probed, have corresponding peaks in the spectrum shown in Figure 8. This indicates that the substrate surface for doped diamond growth is similar to the substrate surface of the undoped diamond growth. Even if the substrate surface cannot be totally characterized by attributing of the features to other known electronic structures, it still allows of differentiation of diamond materials from non-diamond materials. This differentiation makes it possible to distinguish regions which are diamond from the substrate using spectroscopic methods, even when the structures themselves cannot be imaged. This differentiation also provides for the opportunity to establish the location of probable nucleation sights on the substrate prior to growth, as first suggested by Everson and others [17].

C. Comparison of the Interface and Growth Surfaces

The last sample to be examined in this study is a freestanding polycrystalline diamond film. The growth surface of this film, when examined by STM, showed typical structure for extended growth of diamond on silicon. The etched side displayed a very different type of topography and is shown in Figure 12. The ridges that can be seen on the surface are remnants from the scratches that were made on the silicon to increase the nucleation density.

Figures 13, 14, and 15 present the surface DOS of this freestanding film. Figure 13 shows the spectrum taken from the growth side of the freestanding diamond film. The electronic structure most resembles that of the single crystal diamond (Figure 1). It is also close in structure to the doped diamond film grown on silicon but without the steep climb in the surface DOS for positive bias nor the state at 1.8eV.

One could conclude that this sudden rise for positive bias is due to the presence of the silicon substrate, because it is observed for diamond grown on silicon but not for the freestanding

diamond film. This cannot be the cause, since STS measures the surface electronic structure and also because tunneled electrons that reach the Si substrate would be thermalized and would not show the electronic structure.

An alternate explanation is that the sudden rise for positive bias is due to graphitic electronic structures on the surface or in the film. Referring to Figure 5, there is a rise also for positive bias voltages, but it is less steep. The results of Raman spectroscopy of the diamond nuclei and films show that all of the diamond has some sp^2 bonded material with the exception of the freestanding film. For the freestanding film, no sp^2 bonded material was detected. This result illustrates the utility of using STS as a measure of the sp^2 bonded material on the surface of diamond.

Figure 14 provides a clear example of the utility of STS for characterization of the electronic structure of the surface. The STS spectrum of the etched, back side of the freestanding film is shown in Figure 12. The spectrum shows a broad peak centered at -2.2eV, a region of low conductivity between 0.5eV and 2.1eV, and a shoulder extending between 2.2eV and 3.5eV. By comparing this spectrum with those featured in Figures 5 and 5.6, a discovery can be made. Most of the surface DOS is made up silicon carbide-like and graphitic-like structures. In fact, if both the graphite and silicon carbide spectra are added together, the result looks remarkably like the spectrum shown in Figure 14. Since the Si has been etched away, only the interfacial layers remain behind. Several studies have provided evidence for the formation of silicon carbide or other carbon layer as a precursor for diamond growth [32,33,36]. This provides further evidence for the precursor being made up of graphitic and silicon carbide layers.

A contrast between the front and the back sides of the freestanding diamond film are displayed in Fig. 15. The results demonstrate the surface sensitivity of the STS process. Working with a UHV STM, one could map out such an interface on both the physical and electronic levels. Working in UHV, the surface electronic structure could be separated from the structures created by absorbed molecules, and thus a finer level of characterization. Better resolution would allow for surface band structure theories to be applied and tested.

IV. Conclusions.

The structures of Si(100), graphite, single crystal diamond, and SiC were measured to serve as standards. The electronic structures of doped diamond films, undoped diamond nuclei, and doped diamond, all deposited on Si, were all charted. The three appear to be very similar in terms of their STS spectra. The structures of the layers deposited on the substrates during diamond deposition were identified. The etched and growth sides of a freestanding film were found to have different electronic structures, and the etched side provided evidence for precursor layers containing silicon carbide and graphitic carbon. In subsequent research, use of a UHV STM would allow for greater resolution, and actual identification of bonding and surface states.

Acknowledgments

We acknowledge F. Jansen and M. Machonkin of Xerox Webster Research Center for supplying one of the doped films for this study, and W. Zhu, B. R. Stoner and J. T. Glass of the Department of Materials Science and Engineering, NCSU, for providing the freestanding diamond film and the undoped nucleation sample. We also acknowledge Michelle Hartsell of Kobe Steel Research Laboratories, USA for preparing the doped nucleation sample. This study was supported in part by the Office of Naval Research (Contract #N00014-90-J-1707).

References

1. W. G. Eversole, U. S. Patent 3,030,188 (1961).
2. W. A. Yarbrough and R. Messier, Science **247**, 688 (1990).
3. J. C. Angus, Z. Li, M. Sunkara, R. Gat, A. B. Anderson, S. P. Mehandru, and M. W. Geis, in *Proceedings of the International Symposium on Diamond and Diamond Materials, Electrochemical Society Meeting, Washington, D. C.* (Electrochemical Society, New York, 1992), p.125.
4. B. E. Williams and J. T. Glass, J. Mater. Res. **4**, 373 (1989).
5. A. A. Morrish and P. E. Pehrsson, Appl. Phys. Lett. **59**, 417 (1991).
6. B. R. Stoner, G. H. M. Ma, S. D. Wolter and J. T. Glass, Phys. Rev., B **45**, 11067 (1992).
7. R. J. Hamers, R. M. Tromp, and J. E. Demuth, Phys. Rev. Lett. **56**, 1972 (1986).
8. J. A. Stroscio, R. M. Feenstra, and A. P. Fein, Phys. Rev. Lett. **57**, 2579 (1986).
9. F. Iwawaki, M. Tomitori and O. Nishikawa, J. Vac. Sci. Technol., B **9**, 711 (1991).
10. J. J. Boland, J. Vac. Sci. Technol., A **10**, 2458 (1992).
11. R. S. Becker, Proc. Nat. Acad. Sci. **84**, 4667 (1987).
12. R. S. Becker, B. S. Swartzentruber, and J. S. Vickers, J. Vac. Sci. Technol. A **6**, 472 (1988).
13. R. M. Feenstra and A. J. Slavin, Surf. Sci. **251**, 401 (1991).
14. C. S. Chang, I. S. T. Tsong, Y. C. Wang and R. F. Davis, Surf. Sci. **256**, 354 (1991).
15. D. A. Bonnell, G. S. Rohrer and R. H. French, J. Vac. Sci. Technol., B **9**, 551 (1991).
16. K.F. Turner, Y.M. LeGrice, B.R. Stoner, J.T. Glass, R.J. Nemanich, J. Vac. Sci. Technol. B **9**, 914 (1991).
17. M.P. Everson, M.A. Tamor, J. Vac. Sci. Technol. B **9**, 1570 (1991).
18. J. V. LaBrasca, R. C. Chapman, G. E. McGuire and R. J. Nemanich, J. Vac. Sci. Technol. B 9, 752 (1991).
19. T. Takigami and M. Tanimoto, Appl. Phys. Lett. **58**, 2288 (1991).

20. R. M. Feenstra, J. A. Stroscio and A. P. Fein, Surf. Sci. **181**, 295 (1987).

21. N. D. Lang, Phys. Rev. B **34**, 1164 (1986).

22. R. H. Fowler and L. Nordheim, Proc. Roy. Soc. London A **119**, 173 (1928).

23. H. J. Freund, J. Ragozik, V. Dose and M. Neumann, Surface Sci. **175**, 94 (1986).

24. J. A. Kubby and W. J. Greene, J. Vac. Sci. Technol. B **9**, 739 (1991).

25. F. J. Himpsel, J. A. Knapp, J. A. VanVechten, and D. E. Eastman, Phys. Rev. B **20**, 624 (1979).

26. B. B. Pate, M. H. Hecht, C. Binns, I. Lindau, and W. E. Spicer, J. Vac. Sci. Technol. **21**, 364 (1982).

27. F. Iwawaki, M. Tomitori and O. Nishikawa, J. Vac. Sci. Technol., B **9**, 711 (1991).

28. J. J. Boland, J. Vac. Sci. Technol., A **10**, 2458 (1992).

29. H. Fuchs and E. Tosatti, Europhys. Lett. **3**, 745 (1987).

30. A. Selloni, P. Carnevali, E. Tosatti and C. D. Chen, Phys. Rev. B **31**, 2602 (1985).

31. R. J. Nemanich, L. Bergman, K. F. Turner, J. van der Weide, and T. P. Humphreys, in *Proceedings of the 7th Trieste Semiconductor Symposium on Wide-Band-Gap Semiconductors*, edited by C. G. van de Walle, to be published.

32. B. R. Stoner, G. H. M. Ma, S. D. Wolter and J. T. Glass, Phys. Rev., B **45**, 11067 (1992).

33. B. E. Williams, B. R. Stoner, D. A. Asbury, and J. T. Glass, in *Diamond and Diamond-Like Films and Coatings, NATO Advanced Study Institute, Series B: Physics*, edited by J. Angus, R. Clausing, L. Horton, and P. Koidl (Plenum, New York, 1990).

34. Ph. Avouris, I.-W. Lyo, and F. Bozso, J. Vac. Sci. Technol. B **9**, 424 (1991).

35. R. J. Nemanich, L. Bergman, Y. M. LeGrice, and R. E. Shroder, in *Proceedings of the Second International Conference on the New Diamond Science and Technology*, edited by R. Messier and J. T. Glass (Japan New Diamond Forum, Washington, D.C., 1990).

36. J. J. Dubray, C. G. Pantano, M. Meloncelli and E. Bertran, J. Vac. Sci. Technol., A. **9**, 3012 (1991).

Figure Captions

1. STS curve showing the surface density of states for single crystal diamond. The curve is a plot of the normalized differential conductivity versus bias voltage. In this plot, and all subsequent plots, the normalized differential conductivity is labeled as "DOS".
2. Band diagram showing the tunneling spectroscopy process in the case of single crystal diamond.
3. STS curve obtained from the Si(100) surface. The surface was prepared by cleaning with HF.
4. STS curve obtained from the surface of n-type SiC.
5. STS curve obtained from the surface of highly-oriented pyrolithic graphite.
6. STS curve obtained from the surface of a doped polycrystalline diamond film on silicon.
7. STS curve obtained from the surface of an undoped diamond nucleus on silicon.
8. STS curve obtained from the surface of the substrate near an undoped diamond nucleus.
9. Comparison of the STS curves obtained from the surfaces of an undoped diamond nucleus on silicon and an adjoining region of the substrate.
10. STS curve obtained from the surface of a doped diamond nucleus on silicon.
11. STS curve obtained from the surface of the silicon substrate near a doped nucleus after one hour of growth.
12. STM image of the etched side of the freestanding diamond film. This figure shows the ridges caused by the scratches that were made on the silicon surface, which was etched away.
13. STS curve obtained from the growth surface of the freestanding diamond film.
14. STS curve obtained from the etched surface of the freestanding diamond film.
15. Comparison of the STS curves obtained from the growth and etched sides of the freestanding diamond film.

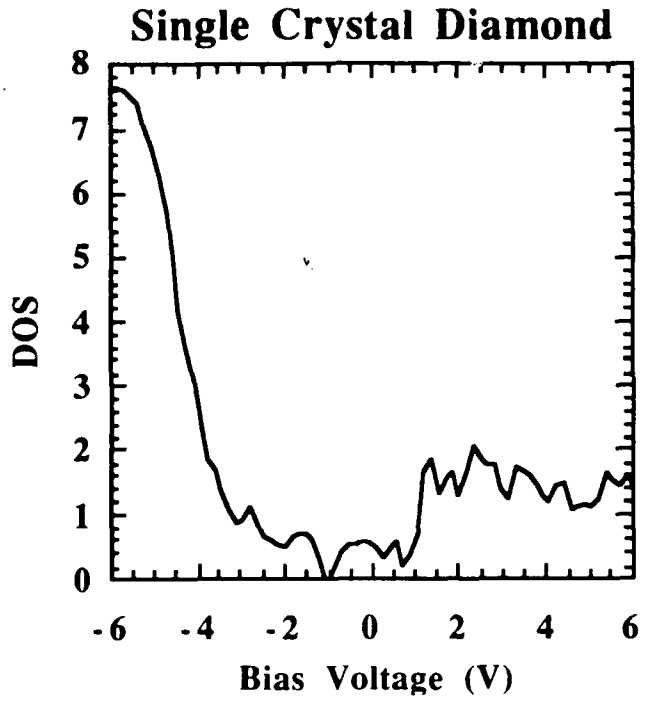

Figure 1

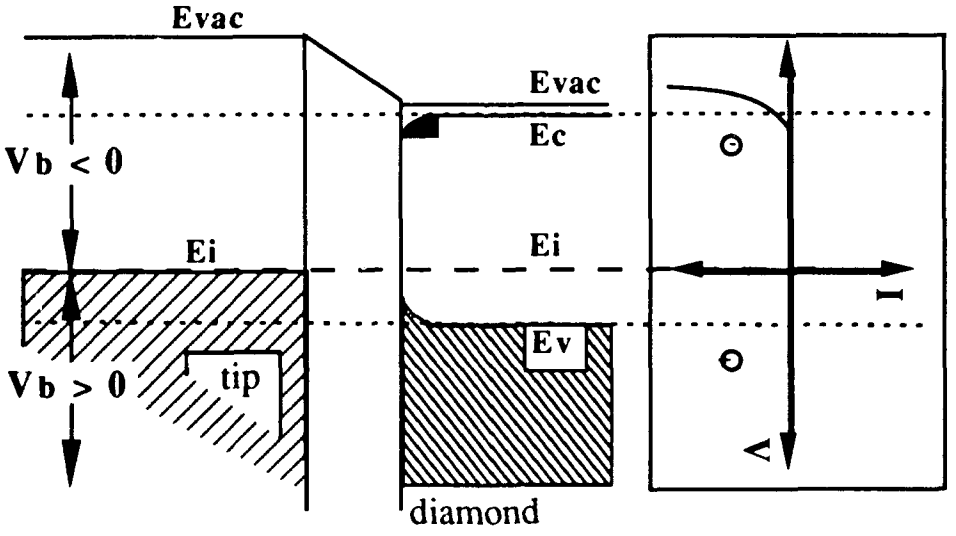

Figure 2

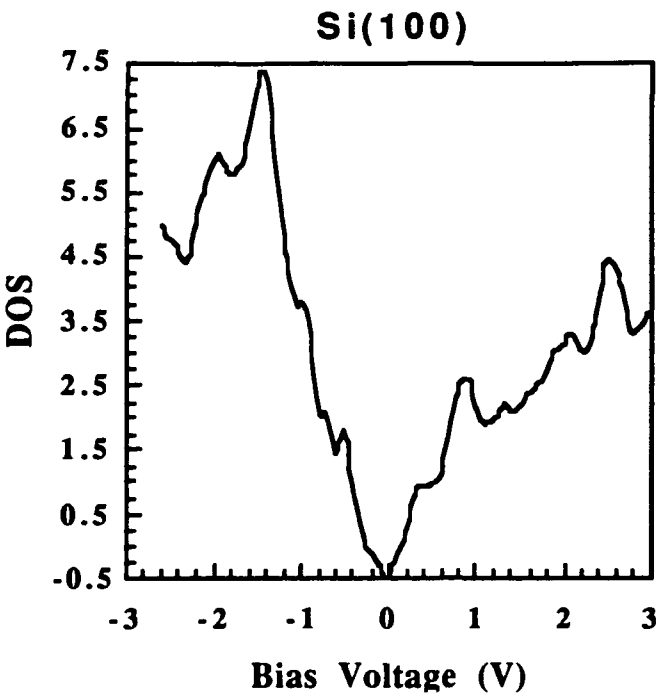

Figure 3

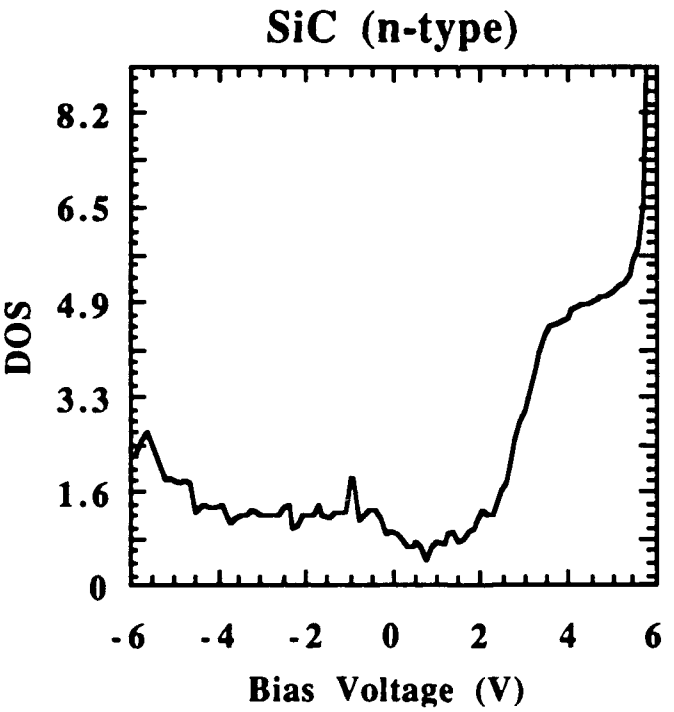

Figure 4

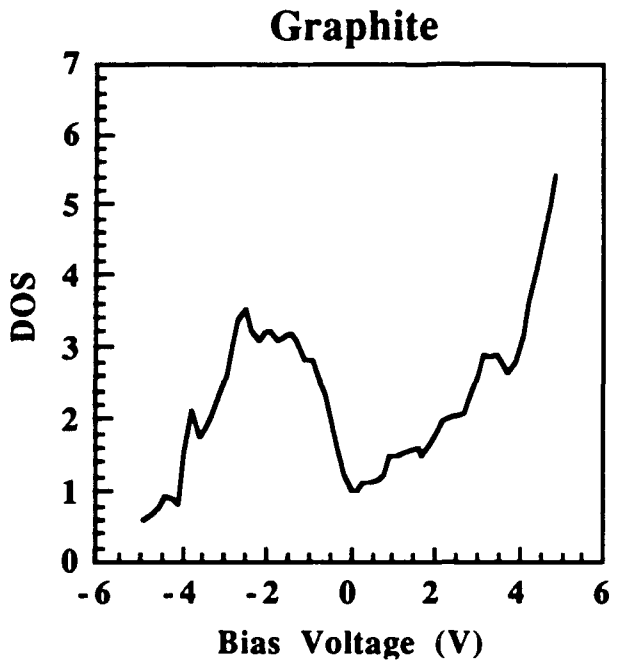

Figure 5

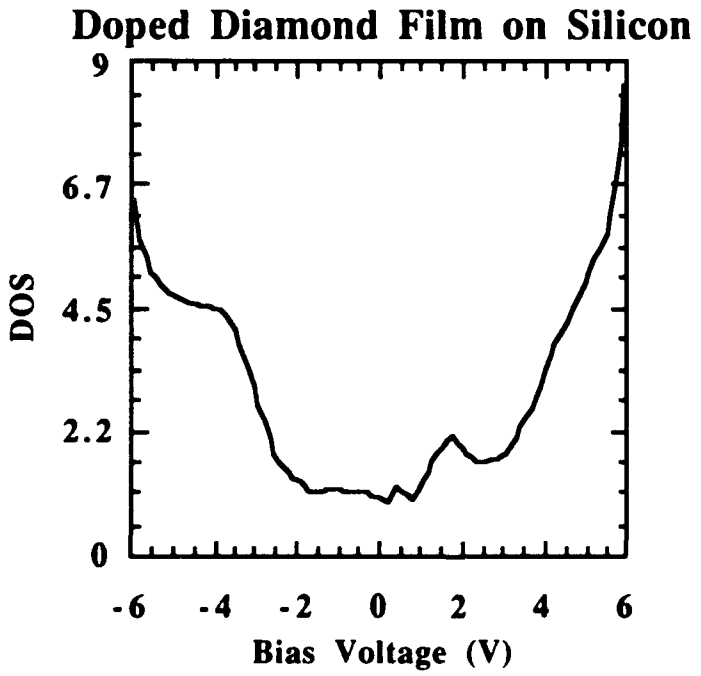

Figure 6

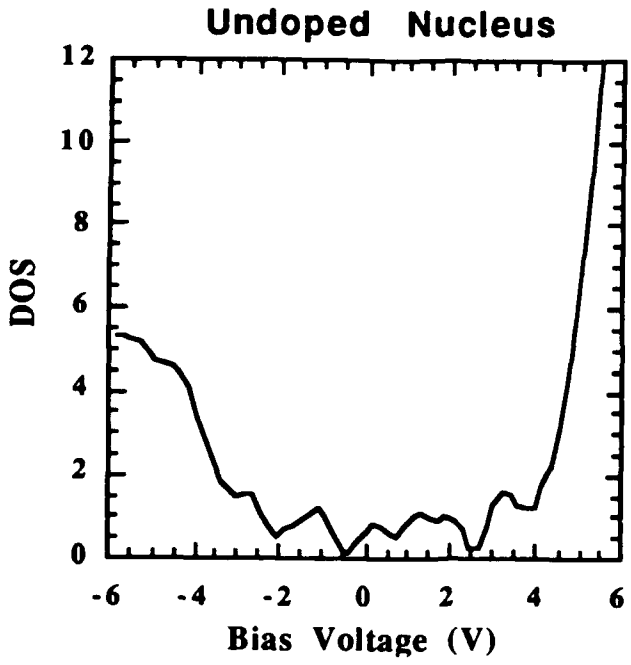

Figure 7

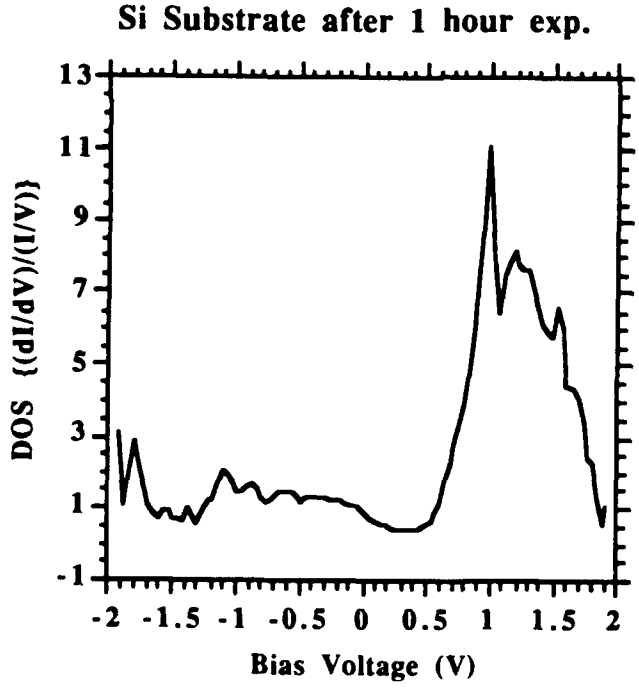

Figure 8

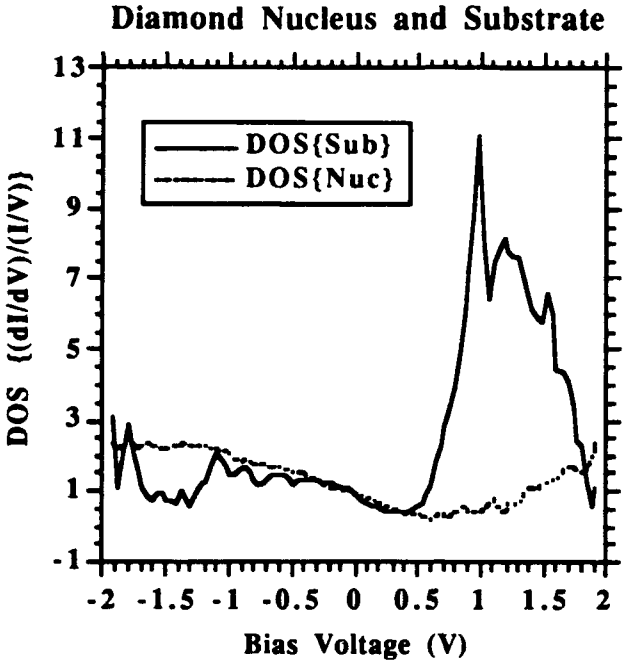

Figure 9

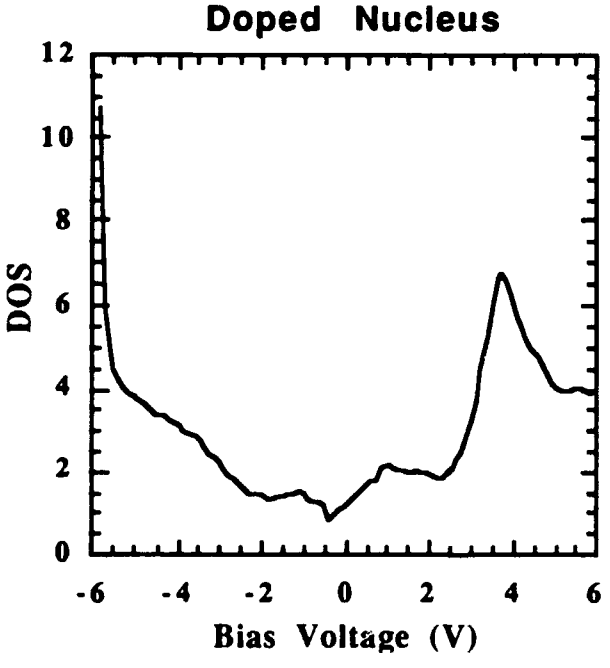

Figure 10

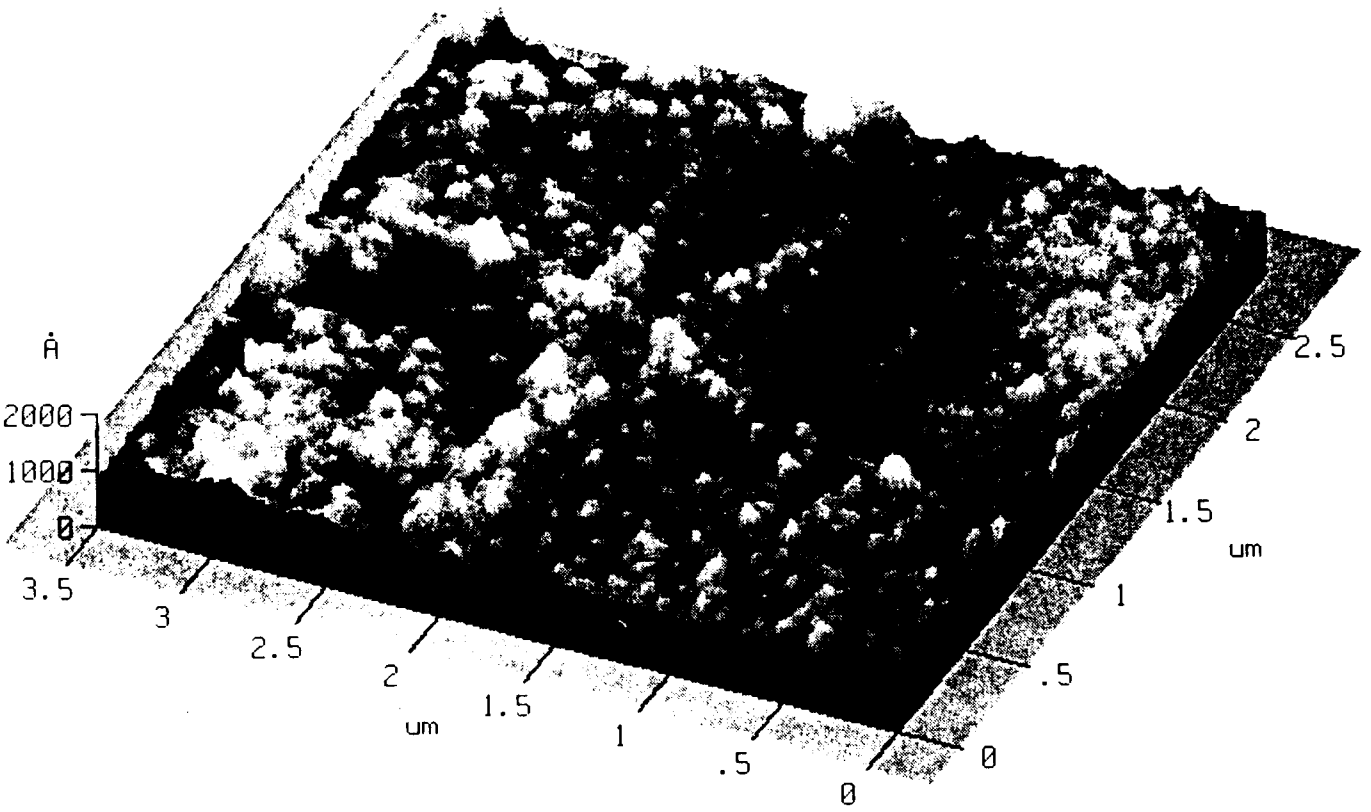

Fig. 12

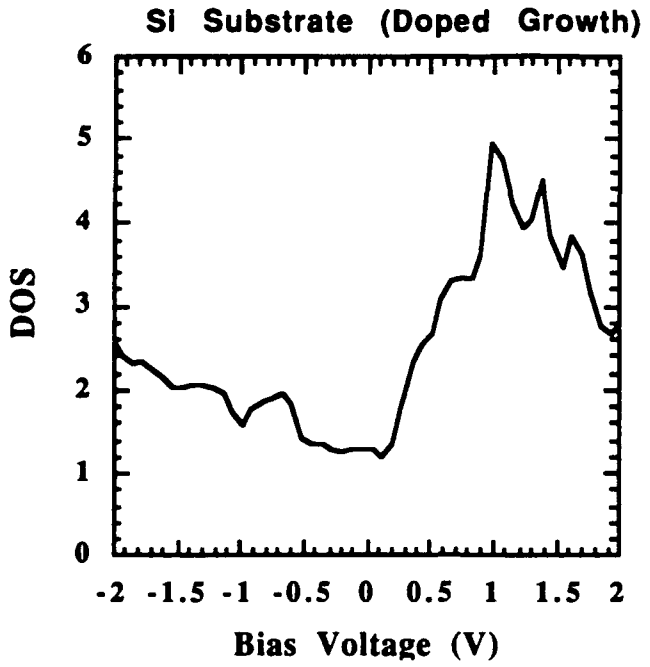

Figure 11

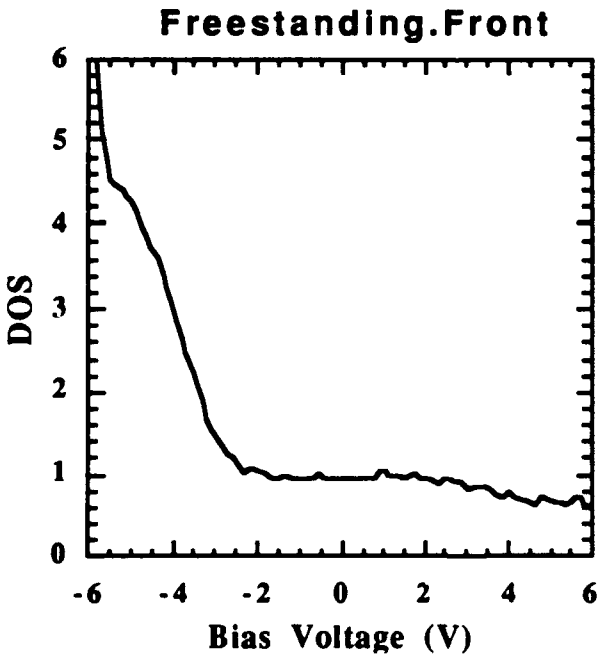

Figure 13

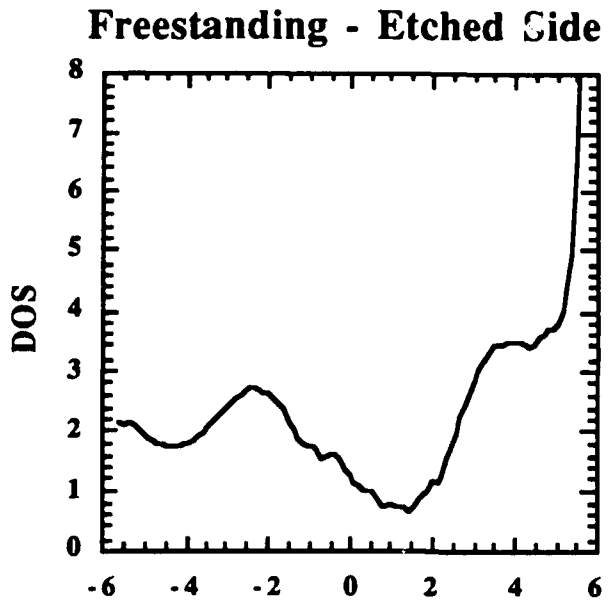

Figure 14

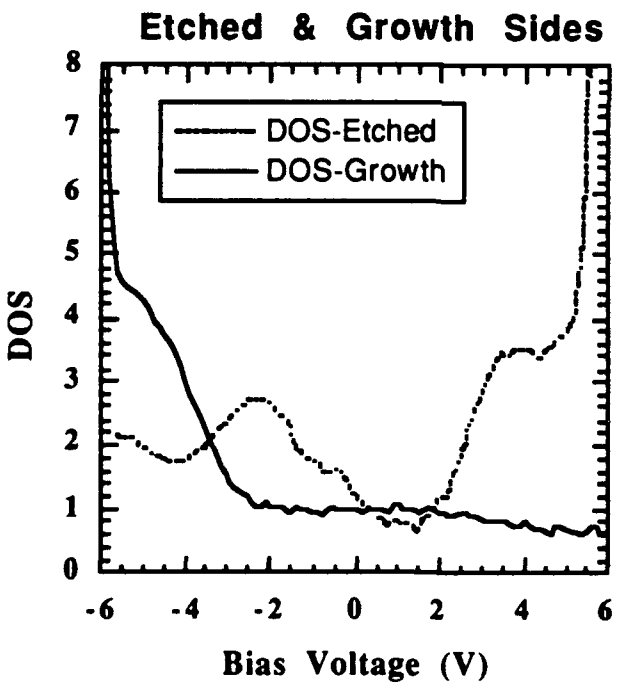

Figure 15

V. Semi-Annual Diamond Report - IST/SDIO/ONR - R.J. Trew 9/1/92

Modeling of Microwave MESFET Electronic Devices Fabricated from Semiconducting Diamond Thin Films

Abstract

The microwave performance of p-type diamond MESFETs is under investigation. A detailed, theoretical model for the device that includes all known physical phenomena of significance is being developed. The model is based upon a full two-dimensional formulation of the appropriate semiconductor device equations. The equations are solved using numerical simulation procedures. Of particular interest in the model formulation is the development of a complete and accurate description of the semiconductor surface between the gate and drain electrodes. Accurate inclusion of the surface effects requires the development of models for both surface conduction and channel breakdown. During the past reporting period the surface breakdown model has been further refined. Also, an activation model has been included so that free charge density as a function of temperature could be determined. The model is currently being tested against experimental data.

I. Introduction

The operation of p-type diamond MESFET's is under investigation. It has been observed that these devices are limited in possible applied drain bias by a gate leakage problem. The gate leakage prevents the application of sufficient drain bias to saturate the current flow in the channel. The inability to achieve full channel current saturation limits the gain that can be achieved with the device.

We have proposed a breakdown mechanism for MESFET's that explains the gate leakage and breakdown phenomena observed in experiments. The new gate leakage and breakdown mechanisms have been formulated and are currently being incorporated into the device model. Initial results of this work are encouraging, although simulation time can be large. We are currently refining the model formulation to reduce execution time so that the model can be used for design investigation.

We have also begun formulation of a JFET modification to the program. This work requires development of a pn junction model to replace the Schottky gate model in the current model. This work is anticipated to serve as a stepping stone to formulation of a heterojunction model that can be applied to diamond heterostructures.

II. Investigation Procedure

The formulation of the surface model for the region between the gate and drain electrodes has continued. In this model the surface of the MESFET is a complex physical system where a periodic lattice of diamond atoms terminate into either free space or another material such as gate metals, other semiconductors, or passivating (i.e., insulating) materials. Typical numerical or analytic models for MESFET's neglect surface effects and only include the first order bulk transport properties in the formulation. First order physics describes MESFET operation in terms of particle conservation equations and particle flux equations which have field, diffusion, and sometimes thermal components. Poisson's equation completes the set by relating the particle and fixed charges within the device to potential. The initial formulation previously reported has been further refined and extended. The model allows for the trapping of negative charge on the surface of the semiconductor in the region between the gate and drain electrodes. The negative charge, in turn, results in a surface depletion region that can penetrate a significant distance into the channel, thereby reducing the cross-sectional area through which current can flow, and reducing the drain current. This phenomenon, although well understood, requires considerable sophistication

in the device model, especially when the time dependence of the traps is included. It is necessary to consider the charging/discharging time of the surface traps since the quantitative density of surface charges will determine the degree of surface depletion. The process is frequency dependent and affects the RF operation of the device.

The model has also been extended to include the thermal activation of dopants. This is necessary since the relatively high activation energy of the impurities results in few free charges at room temperature. For example, at room temperature only about 0.01% of the boron atoms in a p-type diamond MESFET structure may be activated. The model predictions are being compared to experimental data provided by Kobe Steel on their recently reported diamond MESFET.

III. Results

The NCSU MESFET model under development incorporates all dominant physical effects simultaneously. Effects such as electric field or energy dependent carrier mobilities, generation and recombination mechanisms, and thermal effects are being included in the formulation. Formulation of the model is continuing and preliminary predictions on the effects of surface depletion have been obtained.

The diamond MESFET reported at the recent Device Research Conference by researchers from Kobe Steel is being simulated. This device is formed from polycrystalline p-type diamond and demonstrates current saturation. The initial simulation results did not provide satisfactory results and the simulation study is continuing. The initial attempts to simulate the structure resulted in predicted drain currents about 3 orders of magnitude larger than measured. The reasons for the large discrepancy are under investigation. Possible reasons for the errors include: (1) underestimation of the surface depletion phenomenon, (2) neglect of possible substrate trapping phenomenon, (3) errors in determining the free charge density from the activation model, (4) underestimation of parasitic resistance effects,

and (5) underestimation of the charge transport degradation caused by grain boundaries. Each of these areas have been investigated. The surface depletion phenomena could have a significant effect since the high resistivity of the channel semiconductor results in very significant channel depletion due to surface trapping. Charge transport by space-charge-limited flow is likely. An analogous effect occurs at the interface between the conducting channel and the substrate. The combination of surface and substrate trapping could result in much reduced channel current. The activation mechanism has been investigated and is not thought to be a main problem since the activation is fairly well known. Small deviations would produce slight current variations, but this is easily accounted for by adjustments to the activation energy. The increased scattering due to grain boundaries has also been investigated. The grain boundaries introduce additional scattering locations that can significantly reduce mobility and saturated velocity. The largest effect is upon mobility, which for this device is in the range of 1-10 cm^2/V-sec. This phenomenon can account for about one order of magnitude of the discrepancy, but not the three orders of magnitude so far observed. Currently, the effects of large parasitic resistance are being investigated. It is possible that the techniques used to measure the contact resistivity of the source and drain contacts significantly underestimate the actual resistivity. The ohmic contact involves generation of a graphite layer between the ohmic metal and the p-type channel material. Although it was expected that the contact resistivity is in the range of 10^{-3}-10^{-4} Ω-cm^2, it is possible that the actual value is significantly larger. If so, a large source resistance could result and this would, in turn, produce a significantly reduced channel current. It is felt that a large source resistance is a likely contributor to the low magnitude of channel current observed in the experimental data. The model is being modified to investigate the low channel current observed. Since the diamond MESFET has a current capability 3 orders of magnitude larger than actually measured, it is felt that significant improvements will result once the reasons for the low current are determined. The model will be fit to the experimental data to determine the parameters responsible for the low current.

A pn junction gate model is also being formulated for inclusion into the device model. The JFET model will allow investigation of these devices, as well as serve as a foundation for development of a heterojunction model. It is believed that heterojunctions of diamond and other semiconductors, such as cBN, may offer improved performance. The goal will be to increase free carrier density by injecting charge across the heterojunction. The injected charge should be able to make use of the excellent transport properties of the diamond to produce a high current structure.

IV. Conclusions

The operation of a p-type diamond MESFET is under investigation. The investigation is directed towards the development of a physical model for the device. The model is being formulated to include all physical phenomena known to be of significance to device operation. Of particular interest is an accurate simulation of gate breakdown, including both gate tunneling and avalanche breakdown. Also, a thermal activation model has been formulated and included into the model. This model allows calculation of the free charge density in the diamond layers as a function of temperature. Work is under way to simulate the performance of the Kobe p-channel MESFET reported at the recent Device Research Conference. Initial calculations predicted a much larger drain current than actually measured. The reasons for the discrepancies are under investigation. A pn junction gate model is also being formulated so that the operation of diamond JFET's can be investigated.

V. Future Research Plans and Goals

The surface model will be further expanded and refined. The initial formulation is concentrating upon an electron hopping mechanism in which charge conduction occurs by trap-to-trap transfer. Continuum mechanics are being applied to particles in the surface energy bands. The stochastic transfer of particles to adjacent states appears at the

macroscopic level to be continuous, with the effect of the lattice being combined into the effective mass of the particle. Therefore, the particle behaves as if it has an effective mass which is related to the curvature of the appropriate energy band. Charge packets propagate and disperse in a Gaussian shape. The packet moves in time if there is an applied field, and simultaneously disperses due to mutual repulsion of the carriers in the packet. Transport in a disordered medium is markedly different from an ordered semiconductor. The full nature of this is being investigated.

The Kobe diamond MESFET will continue to be investigated in an effort to determine the reasons for the low current measured compared to the simulations. A likely reason for the discrepancy between the simulated and measured data is the source resistance. This phenomenon is under investigation. Also, the effects of surface trapping will be further investigated. It is felt that significant improvements in the drain current may be possible once the reasons for the low value of current measured are understood. Development of the JFET model will also continue.

VI. Distribution List

	Number of Copies
Mr. Max Yoder Office of Naval Research Electronics Division, Code: 1114SS 800 N. Quincy Street Arlington, VA 22217-5000	3
Administrative Contracting Officer Office of Naval Research Resident Representative The Ohio State University Research Center 1960 Kenny Road Columbus, OH 43210-1063	1
Director Naval Research Laboratory ATTN: Code 2627 Washington, DC 20375	1
Defense Technical Information Center Bldg. 5, Cameron Station Alexandria, VA 22314	4